Measuring and Understanding Contact Area at the Nanoscale: A Review

Tevis D. B. Jacobs
Department of Mechanical Engineering and Materials Science,
University of Pittsburgh,
3700 O'Hara Street,
Pittsburgh, PA 15261

Ashlie Martini
Department of Mechanical Engineering,
University of California Merced,
5200 N. Lake Road,
Merced, CA 95343

The size of the mechanical contact between nanoscale bodies that are pressed together under load has implications for adhesion, friction, and electrical and thermal transport at small scales. Yet, because the contact is buried between the two bodies, it is challenging to accurately measure the true contact area and to understand its dependence on load and material properties. Recent advancements in both experimental techniques and simulation methodologies have provided unprecedented insights into nanoscale contacts. This review provides a detailed look at the current understanding of nanocontacts. Experimental methods for determining contact area are discussed, including direct measurements using in situ electron microscopy, as well as indirect methods based on measurements of contact resistance, contact stiffness, lateral forces, and topography. Simulation techniques are also discussed, including the types of nanocontact modeling that have been performed and the various methods for extracting the magnitude of the contact area from a simulation. To describe and predict contact area, three different theories of nanoscale contact are reviewed: single-contact continuum mechanics, multiple-contact continuum mechanics, and atomistic accounting. Representative results from nanoscale experimental and simulation investigations are presented in the context of these theories. Finally, the critical challenges are described, as well as the opportunities, on the path to establishing a fundamental and actionable understanding of what it means to be "in contact" at the nanoscale. [DOI: 10.1115/1.4038130]

1 Introduction

1.1 The Concept of Contact and the Outline for This Review. From a continuum mechanics perspective, the definition of "contact" is a location at which the distance between two bodies is exactly zero. From an atomic perspective, the notion of contact is ambiguous; atoms exert forces on other atoms, which depend on their separation distance and their electronic bonding configuration. In real-world devices and technologies, the concept of *contact area* is relevant for understanding the functional properties of interfaces; yet this quantity is difficult to precisely measure or even define. There has been a significant amount of investigation into this topic in recent years, with major breakthroughs enabled by developments in experimental measurement techniques and simulation methodologies. However, open questions remain related to the fundamental meaning of contact at the nanoscale. There are significant challenges and opportunities in this important field, and further research is needed to develop a comprehensive understanding.

This review paper is focused on contact between nanoscale bodies, called *nanocontacts*. Here, a nanocontact is defined as a contact where the global geometry (ignoring roughness) of one or both bodies has characteristic dimensions that are less than 100 nm. A very common example is the nanoscale tip of the sharp probe that is used in scanning probe microscopy (SPM) and other nanoprobe-based applications, but similarly sized contacts are found in many applications containing nanowires and nanoparticles. Further, it is worth noting explicitly that the dimensions of the *contact* are often much smaller than the dimensions of the bodies.

First, the present section presents the relevance of nanocontacts for practical applications, in fundamental science and as model systems for large-scale contacts. The following two sections focus on approaches that have been used for measuring the contact area between nanoscale bodies using experimental methods (Sec. 2) and atomistic simulation techniques (Sec. 3). In Sec. 4, different theories of nanocontact are presented that have been proposed to describe and predict contact area, with examples of support for each theory from experiments and simulations reported in the literature. Finally, Sec. 5 presents a summary of the review and an outlook for the field, with discussion of critical questions that remain as opportunities for future research.

1.2 Relevance of Nanoscale Contacts

1.2.1 Technological Applications. Understanding and predicting the size of a nanocontact as it forms, evolves, and then separates under load has significant implications for engineering applications—especially in materials characterization; nanomanufacturing; and nanodevices (see Fig. 1). For example, scanning probe microscopy approaches to materials characterization (such as spatial properties mapping [1–6]) rely on knowledge of the tip/sample contact for accurate analysis of properties and for achieving high spatial resolution. Even SPM techniques that do not depend explicitly on the value of contact area (such as electrochemical strain microscopy [7] and piezoresponse force microscopy [8,9]) could be made more quantitative and could achieve better spatial resolution with accurate knowledge and control of the real-time contact area. In nanomanufacturing, there are many tip-based techniques [10] (including scanning anodic oxidation lithography [11], reversible nanopatterning of metal–insulator transitions [12], and thermal scanning probe lithography [13]) where the size of the tip/sample contact determines the resolution of patterned features. Additionally, precise understanding and control of nanoscale adhesion (which is related to the true contact area) are required for contact-based nanomanufacturing techniques, such as nanoimprint lithography [14] and pick-and-place manufacturing [15]. In nanodevices, such as electromechanical devices and switches [16,17], the true area of contact determines current flow in the nanodevice such that the mechanics of the contact determine device properties.

Manuscript received September 7, 2016; final manuscript received March 12, 2017; published online November 2, 2017. Editor: Harry Dankowicz.

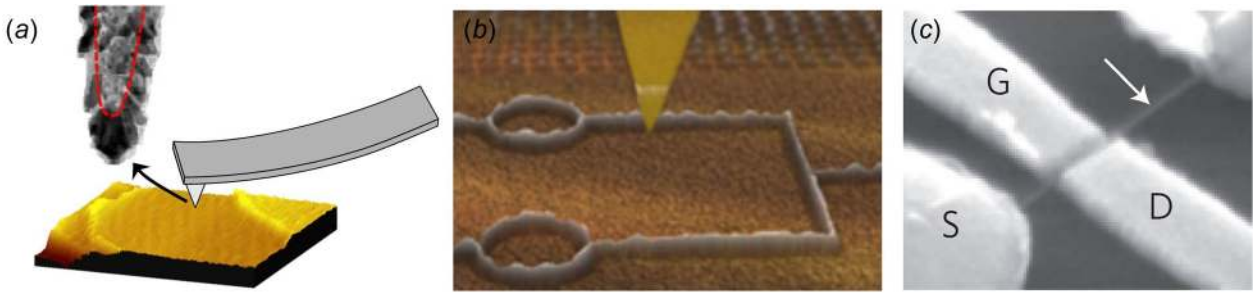

Fig. 1 Technological applications where contact area matters, including (*a*) characterization, (*b*) nanomanufacturing, and (*c*) nanodevices. (Image (*a*) reproduced with permission from Li et al. [18]. Copyright 2011 by American Physical Society. Image (*b*) reproduced with permission from Garcia et al. [10]. Copyright 2004 by American Chemical Society. Image (*c*) reproduced with permission from Loh and Espinosa [17]. Copyright 2012 by Nature Publishing Group)

1.2.2 Scientific Relevance. Understanding the behavior of nanocontacts is also critical from a fundamental science perspective. For example, the atomic-scale origins of Amontons' laws of friction are still being actively explored [19–21], and nanocontacts represent a way to study friction under extremely well-controlled conditions. In some treatments, the friction force is assumed or shown to be proportional to the true area of intimate mechanical contact [20,22], while in others, the true area of contact is not treated as a significant parameter at all [19]. Several small-scale experiments have investigated this question, but it remains difficult to directly and independently measure nanoscale contact area to verify assumptions. As another example, there are significant questions about the transport of electrons and phonons through a nanocontact. While electrical properties of metal nanowires or nanobridges have been well studied (see Sec. 2.1), the same understanding does not exist for arbitrary dissimilar contacts that do not form a wire-like bridge between them. In all cases, it would be beneficial to have a clear, independent understanding of load-dependent contact area in order to measure the relationship between contact geometry and electronic and phononic interactions.

1.2.3 Single Asperities as a Model System for Larger Contacts. Research on individual nanoscale asperities is also motivated by the importance of understanding large-scale contacts between materials. In general, most scientific systems and engineering applications are comprised of more than one material component, and it is often the interface between two materials that determines some element of performance. A key challenge with understanding these interfaces is that most real surfaces, in both engineering applications and in nature, are inherently rough. This means that the overall contact is made up of many smaller contacts between protruding surface features, or *asperities*. Many continuum models exist to describe the effects of roughness on properties (see Sec. 4.2). Some of these models [22–26] rely on the assumption that a rough contact can be described as a statistical collection of individual asperities. Others [27–30] do not make this assumption, but still assume that continuum mechanics applies all the way down to the smallest scales of contact. All of these models would benefit directly from a clearer understanding of contact at the nanoscale, and how parameters like contact area depend on load, material properties, and environmental conditions.

1.3 Defining Contact at the Nanoscale: Apparent and True Contact Area. The size of a contact between two bodies is typically quantified in terms of its area, i.e., contact area. However, even this simple term has multiple possible meanings. The *apparent* (also called *nominal*) contact area is defined by the global dimensions of the bodies in contact, while the concept of *true* (also called *actual* or *real*) contact area is defined by the region(s) where intimate mechanical contact is achieved. On the macroscopic scale, the difference between these is typically attributed to surface roughness, and the true contact area can be more than 100,000 times smaller than the apparent area [31]. These concepts are illustrated schematically in Fig. 2. In a macroscale contact with microscale surface roughness, the true contact area is typically assumed to be the sum of the contact areas of the individual asperities on the surfaces. However, the concept of apparent and true contact area can also be applied to an individual nanoscale asperity. In this case, the definitions are not entirely agreed upon. It was originally assumed (and is implicit in the work of Archard [32] and Greenwood and Williamson [22]) that, for a single-asperity contact, the true and apparent contact area are identical. More recently, atomistic simulations of single-asperity contact [33–36] showed that the contact may still be discontinuous due to atomic corrugation. In view of this, the true contact area can be defined by the atoms that are directly interacting across the interface. The apparent area of contact for an individual asperity might be the area predicted by a continuum mechanics model for those conditions of materials, load, and geometry—or it may be some sort of two-dimensional geometric shape (such as a circle or a polygon) in the plane of contact, which includes all atoms that are in true contact. These definitions are further discussed later in this review.

2 Experimental Methods for Measuring the Area of Nanocontacts

The buried nature of a contacting interface makes direct, accurate measurement of contact area in experiments a substantial challenge. In various investigations, nanoscale bodies were brought into contact under controlled conditions, and then contact area was determined using one of two approaches: (1) measuring one or more properties of the contact as an indirect measurement of contact area or (2) imaging the contact during loading to directly observe the contact size. This section will report the various techniques that have been used for measuring contact area;

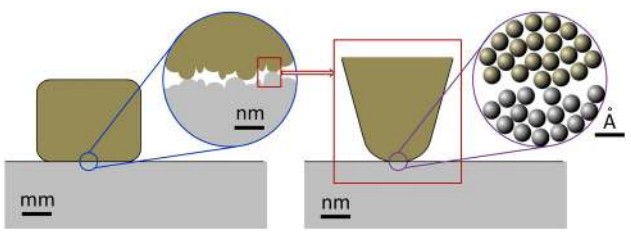

Fig. 2 Conceptual illustration of contact at different length scales, ranging from the macroscale, where the true contact area can be viewed as the summation of the contacts from many asperities in the interface, to the nanoscale, where individual atoms may contribute and the concepts of true and apparent contact area are less well defined

the generalization of measured results for predicting and understanding contact area will be discussed in Sec. 4.

2.1 Indirect Methods for Measuring Nanoscale Contact Area. While contact area is difficult to directly determine, the functional properties of a contact can be straightforwardly measured, even at the nanoscale. Measurable properties that have been used to infer contact size are: electrical and thermal contact resistance; normal contact stiffness; lateral stiffness and friction forces; and the measured surface topography. Examples of each of these are shown in Fig. 3 and described in Secs. 2.1.1–2.1.4.

2.1.1 Measuring Contact Area Using Contact Resistance. As early as 1939, Bowden and Tabor [31] were using electrical contact resistance to understand macroscale contact. It was used to distinguish between the concepts of true and apparent contact area, which were described above. If the contact is assumed to be circular and continuous, with interfacial contaminants or oxides neglected, then it is modeled as an electrical constriction whose size determines the electronic transport through the contact. The exact dependence varies based on the relative size of the radius of the contact compared to the mean free path of an electron in the material, L. This comparison requires knowledge of the mean free path, which can be found in reference texts or can be calculated for metals according to [42]

$$L = \frac{mv_F}{ne^2\rho} \tag{1}$$

where m and e are the mass and the charge of an electron, respectively, v_F is the Fermi velocity, n is the free electron density in the material, and ρ is the bulk resistivity. The value of the electron mean free path in common metals ranges from 4.1 nm in tin to 52.3 nm in silver [42].

When the contact diameter is much larger than the mean free path (the *diffusive* or *Maxwell* limit), the contact resistance is dominated by the spreading resistance on either side of the constriction. The total constriction resistance (which is twice the spreading resistance on each side) varies linearly with the contact radius a according to [42]

$$R_{\text{contact, diffusive}} = \frac{\rho}{2a} \tag{2}$$

If the two materials are dissimilar, then ρ is replaced by $(\rho_1 + \rho_2)/2$ where the subscripts 1 and 2 designate the two materials in contact. When the contact diameter is much smaller than the mean free path of an electron, the contact resistance is given by [42]

$$R_{\text{contact, ballistic}} = \frac{4\rho L}{3\pi a^2} \tag{3}$$

In the intermediate regime, where $L \sim a$, a linear combination of the two is used [42]

$$R_{\text{contact, intermediate}} = \Gamma\left(\frac{\rho}{2a}\right) + \frac{4\rho L}{3\pi a^2} \tag{4}$$

where Γ is a function of L/a, which varies from 1 to 0.694.

The equations above are often referred to simply as the *electrical contact resistance*. In the case of self-mated contacts in vacuum, which form a spontaneous wire-like bridge, this is the only source of electrical resistance from the contact. However, in the more general case of dissimilar materials that may contain surface layers of modified composition (e.g., oxides or contaminants), there is an additional contribution to the resistance that is measured across the interface. For instance, a thin insulating film will require electron tunneling, and will severely limit current flow. The spreading

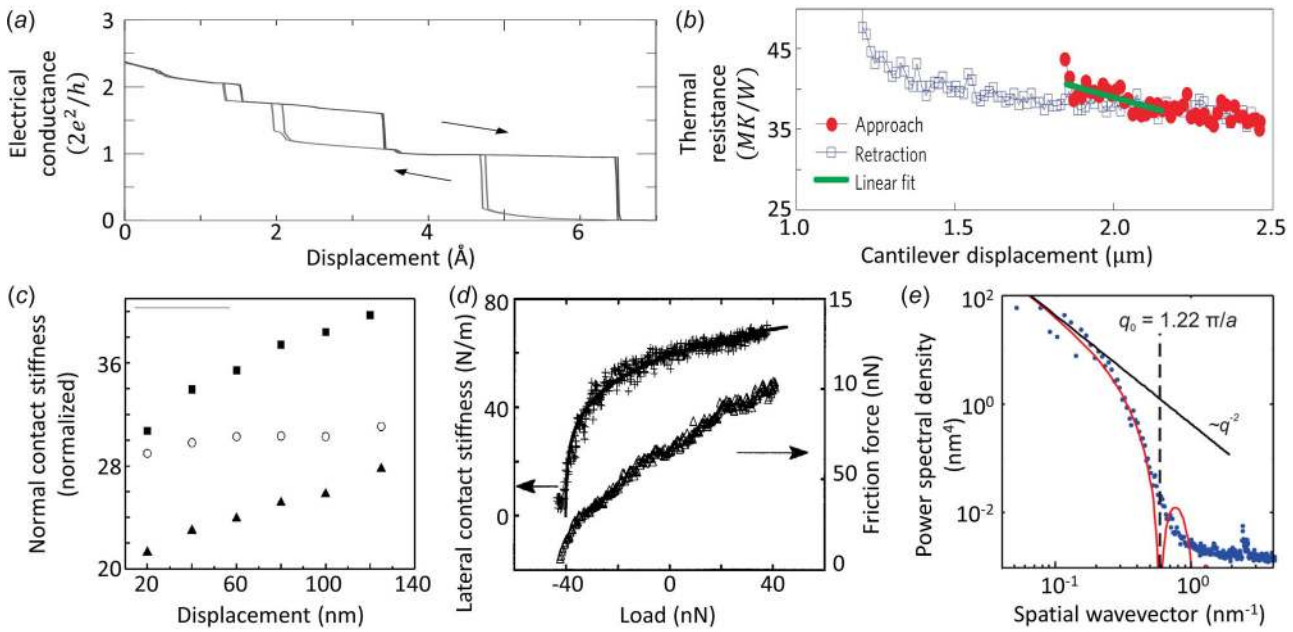

Fig. 3 Various property measurements have been used as indirect measures of contact area. (*a*) The electrical conductance of an atomic-scale gold contact was measured at a temperature of 4.2 K. Reproduced with permission from Agrait et al. [37]. Copyright 2003 by Elsevier. (*b*) The thermal contact resistance was measured between a flattened silicon probe tip and a tetrahedral amorphous carbon surface. Reproduced with permission from Gotsmann and Lantz [38]. Copyright 2013 by Nature Publishing Group. (*c*) Normal contact stiffness was measured for three different silicon SPM tips against a fused quartz substrate. Reproduced from Kopycinska-Müller et al. [39]. Copyright 2006 by Elsevier. (*d*) Both the lateral contact stiffness of the sticking contact and the friction force of the sliding contact have been measured for a silicon nitride tip against a muscovite mica surface. Reproduced from Carpick et al. [40]. Copyright 1997 by American Institute of Physics. (*e*) The topography of a polymer surface has been measured and used to compute the power spectral density of the surface; the reduction in resolution at small wave vectors is attributed to the size of the contact. Reproduced with permission from Knoll [41]. Copyright 2013 by American Chemical Society.

contribution to resistance and the material contribution to resistance can be viewed as a system of resistors in series, and therefore can be summed to compute the total value that will be measured. If the contributions are expected to be very different, the largest value of resistance will dominate the overall system and can be used as an approximation of the total resistance across the interface.

2.1.1.1 Electrical contact resistance measured using mechanically controllable break junctions. There has been extensive characterization of the electrical properties of ultrasmall contacts of gold and other metals (as reviewed in Ref. [37]). A common method for studying these contacts employs *mechanically controllable break junctions*. In these, a small metal wire is pulled to the point of breakage, typically under ultrahigh vacuum and near-zero temperature. The two sides are then brought slowly back into contact while measuring the electrical transport. The two opposing sides are thus matched and unpassivated and meet at an extremely small point. In many cases, they spontaneously weld to form a nanojunction, and further deformation (in compression or tension) changes the electrical conductance through this narrow neck. Many investigations have precisely measured conductance through these atomic-sized contacts [37]. The measured contact conductance (the inverse of resistance) is quantized and these conductance jumps can be interpreted as "the contact changing size by approximately the area of one atom" [37].

Because these tests form a narrow wire-like bridge, they provide an excellent way to measure the contribution to resistance from the constriction. However, because these break junctions are ultraclean, self-mated, and geometrically and crystallographically matched, they may be unrepresentative of typical nanocontacts. In the more common case, the bodies forming a nanoscale contact will not be commensurate, will be oxidized or otherwise passivated, may be of dissimilar materials, and often experience diffusion and environmental interactions.

2.1.1.2 Electrical contact resistance measured using scanning probe microscopy. Because of the versatility of SPM, it has been very widely used to characterize surface and material properties and to create well-controlled nanoscale contacts. In SPM, the materials, size, shape, and environmental conditions of the contact can be customized, and it can therefore be a very accurate representation of nanocontacts in technological applications. Several investigations [43–46] have measured the resistance through the tip/sample contact as a direct measure of contact area, assuming only a spreading contribution to resistance (i.e., Eq. (3)). One investigation [47] showed qualitatively the effect of the materials contribution to resistance. More recently, a method was demonstrated to quantitatively treat the contribution of an oxide using the Fowler–Nordheim tunneling model [48]. Fitting the model to measured data enables the calculation of what the authors call an "electrical contact area."

2.1.1.3 Thermal contact resistance measured using scanning probe microscopy. There has been limited investigation of thermal contact resistance as an additional method for measuring the contact size. Many of the same concepts apply between electrical and thermal contact resistance, except that heat can be carried by electrons and phonons, which will have different mean free paths and exhibit different scattering behavior. Gotsmann and Lantz [38] have measured thermal contact resistance between a flattened silicon SPM tip and a tetrahedral amorphous carbon surface as a function of load and tip size. The results are fit using a model that assumes quantized thermal transport through individual atomic regions such that the measured thermal conductance scales with the true area of contact.

2.1.2 Measuring Contact Area Using Normal Contact Stiffness. In scanning probe microscopy, the cantilever can be actuated statically or dynamically to measure the force–displacement relationship, the derivative of which yields the instantaneous stiffness of the system [49]. The total system stiffness can be mechanically analyzed as springs in series. By mathematically accounting for the stiffness of the cantilever and other contributions from the system, the stiffness due to the contact itself can be computed. The stiffness of the contact is a function of the mechanical properties of the materials in contact, and also of the size of their contact. Prior investigations have assumed smooth spheres in linear-elastic contact and applied the Hertz model (discussed in Sec. 4.1) to describe the contact stiffness k_{contact} as [50]

$$k_{\text{contact}} = \frac{\partial F}{\partial d} = 2aE^* = \frac{2}{\sqrt{\pi}}E^*\sqrt{A} \tag{5}$$

where F is the force, d is the distance, A is the area of the contact, and E^* is the effective elastic modulus. The effective elastic modulus is a function of the elastic modulus, E, and Poisson's ratio, ν, of each of the two materials: $E^* = [((1-\nu_1^2)/E_1) + ((1-\nu_2^2)/E_2)]^{-1}$. Therefore, in this model, the stiffness is directly proportional to the contact radius and thus directly proportional to the square root of contact area. It has been shown [51,52] that Eq. (5) applies to all smooth, rigid, rotationally symmetric bodies in elastic contact. For larger loads, and other prismatic bodies (such as a pyramid or triangular prism), only a slight modification is required [53]

$$k_{\text{contact}} = \frac{\partial F}{\partial d} = \beta 2aE^* = \beta\frac{2}{\sqrt{\pi}}E^*\sqrt{A} \tag{6}$$

where β is a correction factor that is near unity, but can vary up to about 10%. As with contact resistance, there may be additional contributions to stiffness due to materials factors, including different mechanical properties of oxide and/or contaminant films, and also the stiffness of interatomic interactions across the actual interface. None of these is included in Eqs. (5) and (6). Unlike resistors in series, to compute the total stiffness of a system of springs in series requires summing the inverses of the original components and inverting the result. Therefore, it is the lowest value that will have the dominant contribution.

Under these assumptions, force–distance measurements taken with the SPM have been analyzed to extract the contact area [54]. Also, techniques have been developed to dynamically oscillate a cantilever (such as atomic force acoustic microscopy [1,2,55,56]) to determine the instantaneous stiffness at a certain load, and/or to use multifrequency oscillation to collect data using multiple resonances simultaneously [57]. The majority of these techniques are used for modulus measurement and mapping—under the assumption that the tip's "shape function" ($A_{\text{contact}} = f(d)$) can be precalibrated on a reference material. However, if the mechanical properties of the material are known or assumed, then contact stiffness can be used as an indirect measure for the contact area [39,45].

2.1.3 Measuring Contact Area Using Lateral Contact Stiffness and Friction. Measurements of lateral forces have also been used as an indirect measure of contact area. For a *sticking* contact, for which sliding has not yet initiated, the lateral contact stiffness can be computed as the derivative of the lateral force–displacement curve (in direct analogy to the normal stiffness, discussed in Sec. 2.1.2). The lateral stiffness of a Hertzian contact is given by [58]

$$k_{\text{contact,lateral}} = 8aG^* \tag{7}$$

where G^* is the effective shear modulus, given by $G^* = [((2-\nu_1)/G_1) + ((2-\nu_2)/G_2)]^{-1}$. This has been applied to scanning probe microscopy measurements of lateral stiffness to determine contact area [45,46,59]. Just like normal stiffness, there will be additional contributions to lateral stiffness due to materials factors, such as the interatomic interactions, and those contributions can be even more significant for lateral stiffness [60]. Further, lateral contact stiffness is typically much smaller than the normal stiffness [61], and it has been reported that lateral stiffness may actually be unrealistically small for nanoscale contacts [34,62]. Equation (7)

can be modified for a *partially slipped* contact [63–65], in which some region along the perimeter has slipped to relieve the stress singularity that is predicted by continuum mechanics [66] while the central region is still static. This situation has been explored experimentally with larger contacts [67].

For *sliding* contacts, the behavior is governed by sliding friction and dissipative forces, so the concept of lateral stiffness no longer applies. Here, it is often assumed that the friction force F_{friction} is directly proportional to the true contact area, according to the assumption originally proposed by Bowden and Tabor [31], with a constant of proportionality that is equal to the shear stress τ of the interface. In this case, the area of contact can be computed directly from lateral force measurements

$$F_{\text{friction}} = \tau A \tag{8}$$

In this way, the contact area has been directly extracted from quantitative sliding friction tests [59,68]. There is an excellent body of investigation into the connection between area and friction for atomically flat surfaces (as reviewed in Ref. [69]). Yet it is not yet clear how to apply these insights to the general case of curved nanocontacts.

2.1.4 Measuring Contact Area Using Topography Measurements. A novel way to determine contact area was devised by Knoll [41] for use on hard/soft contacts. For a soft polymer substrate where the statistical roughness was already known, the "blurring" of the measured topography was quantitatively connected to the area of contact. Because the soft polymer conforms to the hard scanning tip, the polymer's topography cannot be locally sampled on scales smaller than the contact area. Thus, the tip/sample contact is assumed to act as a moving average filter for surface topography. The power spectral density of the topography (which is the square of the Fourier transform [70,71] and which decomposes the topography into contributions from different size scales) shows that there is a decay in the contribution to roughness at the small scales. By treating the measured topography as a convolution between the actual surface roughness and the shape of the contact, the measured power spectral density can be fit to determine the contact size [41].

2.1.5 Complications With Indirect Measures of Nanoscale Contact Area. For all indirect measurements of contact area using contact properties, a model must be used to extract the contact area from the measurements. These models rely on significant assumptions about the materials, properties, and shape of the contact, which are discussed in more detail in Sec. 4. Many of these methods assume that the bodies in contact have the shape of a smooth well-defined geometric function (e.g., sphere, rotationally symmetric power-law, etc.), and therefore the area of contact is a single continuous surface. To a certain extent, this type of shape assumption can be supported through careful characterization of the contacting bodies using electron microscopy before and/or after testing (see Ref. [72] and references therein for more details). However, surface roughness on either or both bodies can contribute to the formation of a multi-asperity contact, in which case the direct application of the above models is not straightforward.

For spreading contact resistance in the ballistic regime and for sliding friction, one might make the assumption that a multi-asperity contact behaves as a system of resistors or superposed forces, respectively. In these cases, a multi-asperity contact can still be analyzed with the same type of model. For N individual resistors, the total resistance R_{tot} will still be inversely proportional to the total true area of contact, as follows:

$$R_{\text{tot,ballistic}} = \left(\sum_i^N \frac{1}{R_i}\right)^{-1} \propto \left(\sum_i^N A_i\right)^{-1} = {A_{\text{tot}}}^{-1} \tag{9}$$

Likewise, for sliding friction, under the assumption that the friction force is directly proportional to area, the forces from individual contacts can be summed such that

$$F_{\text{tot,friction}} = \sum_i^N F_i = \tau \sum_i^N A_i = \tau A_{\text{tot}} \tag{10}$$

However, even under these assumptions, the variation of contact area with changes in applied load will be very different for multi-asperity contacts as compared to single-asperity contacts. For instance, the Hertz model predicts a sublinear increase in contact area with load (see Sec. 4.1), while multi-asperity contacts are typically modeled with a linear dependence of contact area on load (see Sec. 4.2). Further, for a multi-asperity contact, Eq. (9) will cease to apply if the individual contact radii should exceed the electron mean free path such that the spreading resistance becomes important.

In the case of a multi-asperity contact, the contact area cannot be determined from the contact stiffness (normal or lateral). The total stiffness of a system of springs in parallel will combine additively. Under the assumption of well-behaved (e.g., circular) contact spots, where $A \propto a^2$, then

$$k_{\text{tot}} = \sum_i^N k_i \propto \sum_i^N a_i \propto \sum_i^N \sqrt{A_i} \tag{11}$$

The sum of individual contact diameters has been termed the *contact length* [73]. Because the individual contacts will vary in size, nothing can be said about the total contact area from the sum of the radii of the contacting spots. Electrical and thermal contact resistance in the diffusive regime will also scale with contact length for multi-asperity contacts. Finally, the method of topography measurements (Sec. 2.1.4) also will not work to determine contact area in the multi-asperity regime because the measured topography represents the convolution of the actual topography with multiple individual contacts of unknown size.

An additional complication of many experimental measurements is the effect of capillarity on nanocontacts. For tests conducted in an ambient environment, water is adsorbed on the surfaces of both bodies and water also exists at a certain partial pressure in the intervening gases. The presence of the water can alter contacts in a variety of ways. First, for a single, smooth contact, water will add an additional adhesive component due to surface tension and the Young–Laplace effect. This acts as an additional load, and can increase the area of solid–solid mechanical contact beyond what would be expected for a dry contact. Second, the fluid will add some additional area, surrounding the solid–solid contact, which is in solid/fluid/solid contact. This will likely add additional channels for electrical or thermal transport, which will alter the measured contact resistance. Third, during the formation of the contact, it has been shown [74] that water can exhibit strong confinement effects at the nanoscale. Before the last few monolayers are squeezed out, they may add an additional component to the stiffness and may prevent intimate contact between the solids. For bodies that contain surface roughness, it is even less clear how to account for the effect of capillarity on contact, and it will likely depend on the details of topography and on the models that are assumed.

2.2 Direct Methods of Measuring Contact Area Using Imaging

2.2.1 Nanocontacts Explored Using Transmission Electron Microscopy. For *macroscale* contacts, one or both bodies can be made transparent and the contact can be directly visualized using reflected or transmitted light through one of the bodies [75–77]. This yields a measure of contact area at the scale of the microscope resolution, but cannot give information about finer scales. The same approach cannot be directly applied to nanocontacts because of limits on the lateral resolution of light. Instead, nanocontacts have been examined using side-view in situ electron microscopy techniques. Gold nanojunctions, similar to those investigated as mechanically controlled break junctions, have

been studied using direct electron imaging in a transmission electron microscope (TEM), as shown in Figs. 4(*a*)–4(*c*).

The deformation of the spontaneously welded neck has been directly observed during compression and tension [81–83], as has the thinning to an atomic chain before separation [84,85]. Similar necking and wetting-type behavior have been observed for large (but still nanoscale) contacts of gold [78]. A separate microelectromechanical systems-based setup has been used to directly observe contact upon adhesive and lateral loading of this type of welded junction [86,87].

In in situ TEM experiments designed specifically to study nanocontacts, the load resolution of SPM was established in the TEM to investigate dissimilar contacts that do not undergo spontaneous welding [88]. This apparatus has been used to quantitatively characterize the out-of-contact geometry of the SPM tip, as well as to measure the corresponding adhesion [89–91], wear [88], and electrical [80] properties. These studies show that, in the general case, there is not fusion of the opposing bodies, but instead, the original interface remains distinct (as shown in Fig. 4(*d*)). In all cases, in situ TEM provides a way to measure the geometry of the bodies, as well as their structure, and composition. During contact, side-view images can be used to compute the diameter of the contact and, under certain assumptions, its contact area.

2.2.2 Complications With Direct Measures of Nanoscale Contact Area. Direct assessment of contact area eliminates the need to assume a functional dependence of a measured property on contact area (which requires significant assumptions about the shape, size, composition, and structure of the bodies in contact). However, the in situ experiments add their own constraints and assumptions. First, the measurements are typically slow and time- and resource-intensive, which precludes performing a very large number of repetitions for statistical analysis. Second, to be imaged in the TEM, the samples must be thin enough to be electron transparent (less than approximately 100 nm in thickness) and conductive enough to avoid significant charge build-up under the electron beam [92]. Third, the energetic electron beam used for imaging can inadvertently change the behavior of the materials under study: changing their mechanical properties [93,94], or decomposing or contaminating the material [92]. Fourth, for non-welding contacts, the measurement of the contact diameter is limited by imaging resolution and TEM artifacts, as well as by apparent overlap between the contacting bodies due to slight out-of-plane shifts. Fifth, only a 2D projection of the contact is visible in the TEM and the ability to tilt is typically limited. Therefore, assumptions must be made about the shape and extent of the contact size in the direction parallel to the imaging beam.

3 Simulation-Based Methods for Measuring the Area of Nanocontacts

Experimental measurements of nanocontacts can be complemented by atomistic simulations, where each atom in the tip apex and near-contact substrate material is modeled explicitly. Such simulations can provide information about the origin of experimentally measured properties and trends, and about what happens in the "buried interface" between the tip and substrate as the contact forms, evolves, and separates. This section first reviews methods that have been used for modeling nanocontacts and then describes how those simulations have been used to calculate contact area.

3.1 Simulation Methods. The most commonly used atomic-scale simulation methods for studying nanocontacts are simulations based on empirical models (also called potentials or force fields). These models describe the energetic interactions between atoms as a function of their type and distance from one another using empirical expressions, thereby enabling simulation of larger systems than would be accessible with first-principles calculations. Using empirical models, nanocontacts have been studied using two types of simulations: molecular statics and molecular dynamics. The former uses numerical algorithms to find the nearest minimum-energy configuration. Molecular statics simulations are very fast and efficient, but the minimum energy configuration identified may be a local, as opposed to global, minimum energy state. In molecular dynamics, the atom positions evolve through time, with their movement determined by Newton's laws computed using the empirical potential and the simulation time-step. This is a more computationally expensive approach than molecular statics, but it allows the system to sample a larger set of configurational spaces and enables the simulation to capture dynamic processes. Both approaches have been used effectively to explore nanocontacts.

Typically, atomistic simulations of nanocontacts have consisted of a model of the apex of an SPM tip and the near-contact substrate material. Such models are often designed to capture the key aspects of a specific experimental system. The most important features of the model in terms of accurately capturing the key physics of a nanocontact are: (i) the atomic interactions within and between the tip and substrate that capture materials and material properties, (ii) the size, shape, and other features of the tip and substrate, and (iii) operating conditions including load and, in the case of molecular dynamics, speed, and temperature. This section reviews the most common approaches for modeling each of these aspects. Note that this review is focused on simulations of single-asperity contact and does not include methods for modeling contact between nominally flat surfaces with roughness.

3.1.1 Defining Atomic Interactions. The size of a nanocontact is significantly affected by the elastic response of the bodies in contact. This means that the atomistic model must accurately describe the materials in the tip and the substrate to correctly capture nanocontact behavior. Materials are typically described in these simulations by an empirical model of the energetic interaction between the atoms in the system, and there are different empirical models applicable to different types of materials. The simplest is a generic potential, such as Lennard–Jones, where the model is not expected to capture real material properties (e.g., elastic or thermal properties), but can give insight into general trends of nanocontact behavior [33,34,95]. Such models are typically very computationally efficient, enabling large-scale systems to be modeled in a relatively short amount of time. Alternatively, empirical models have been used, which are specifically designed to capture the interactions within a given material of interest. This can be challenging due to the wide range of materials from which tips and substrates can be made (or coated). Further, accurate models of some materials can be very computationally expensive, limiting the size of the system that can be studied. However, realistic material models are needed to accurately model a specific experimental measurement. Most nanocontact simulations of real materials have focused on metallic, silicon-based, or carbon-based materials. Metals without oxide and in a vacuum have been modeled accurately and relatively quickly using the embedded atom method (EAM) [96,97], making this an ideal material for simulation study. However, many scanning probe experiments have been performed with carbon- or silicon-based systems. Such materials have covalent bonds and are best described by potentials that include the bond order of atoms and so capture the formation and breaking of covalent bonds. Examples of reactive potentials used in nanocontact studies include Tersoff [98] for silicon-based materials and AIREBO [99] for carbon-based materials.

Nanocontact behavior is determined by the response of the materials within the tip and substrate, as described in the previous paragraph, but also the strength of the interactions between the tip and substrate. If the tip and the substrate are the same material, or the assumption is made that there is material transfer after the first contact such that subsequent contacts occur between the same material, then whichever potential is chosen to capture interactions within the tip, and substrate will also be used to describe their interaction. However, if the tip and substrate are different, as is often the case in an SPM context, the model must include a

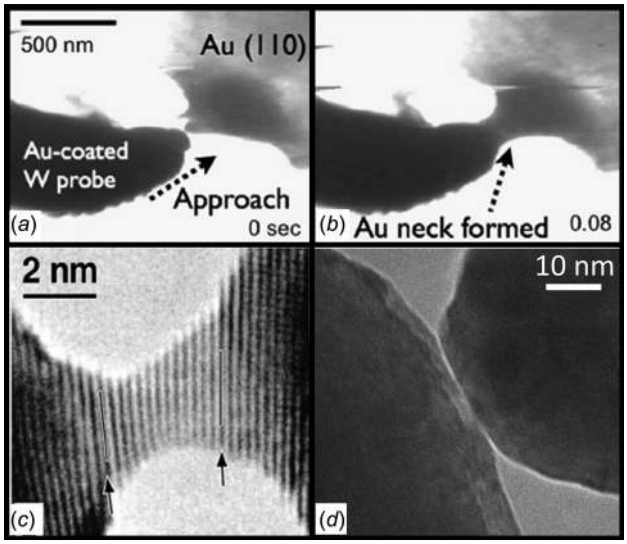

Fig. 4 Electron microscopy has been used to image nanocontacts. Panels (*a*) and (*b*) show the spontaneous welding of a gold nanojunction. Images reproduced with permission from Merkle and Marks [78]. Copyright 2008 by Elsevier. Panel (*c*) shows a separate gold nanobridge, prior to failure in tension. Image reproduced with permission from Rodrigues et al. [79]. Copyright 2000 by American Physical Society. Panel (*d*) shows a dissimilar nanocontact (Pt/Ir on W) that does not spontaneously weld but instead the original interface remains distinct. Image reproduced with permission from Alsem et al. [80]. Copyright 2016 by Cambridge University Press.

cross potential that describes the interactions between dissimilar atoms. If the tip and substrate are similar material types, then the cross-potential may already be well defined. For example, EAM potentials that accurately describe the interactions between many different metals are available [100]. However, in some cases, the best potential form for the tip is not the same as that for the substrate. For example, a metal-coated tip may be modeled using EAM while the graphite substrate on which it slides is best modeled using AIREBO. In this case, researchers often rely on a generic potential to describe tip–substrate interactions [101,102]. If experimental pull-off force or work of adhesion data is available for the system being modeled, the generic potential parameters may be tuned to match the experiments [103]. Specifically, the strength of the interaction is adjusted until the simulation-calculated pull-off force or work of adhesion is matched to that measured in a corresponding experiment.

3.1.2 Defining Model Size, Shape, Crystallinity and Surface Features. Once the interaction models are defined, the next step is typically to create the initial configuration of the tip apex and near-contact region of the substrate. The geometry of the contacting bodies plays a critical role in determining the behavior of a nanocontact and is therefore important to model accurately. Often, one of the bodies is modeled as ideally flat, based on the assumption that one nanoscale body is smaller than the other, and that the larger body can be reasonably approximated as flat. Thus, the design focus for the model geometry is often on the body with the smaller radius of curvature, which, in the case of an SPM contact, is the nanoscale apex of the probe. In cases where a TEM image of the tip is available, the model is created such that it captures the geometry of the TEM profile as closely as possible (see Fig. 5). One approach to extrapolate the 2D profile to a 3D volume is to use the method of disks [88,104]. In this method, the width of the tip at each vertical position on the 2D TEM image is assumed to be the diameter of a circle that defines the 3D geometry of a surface [103]. A more common alternative is the simpler approach of approximating the tip as a well-defined geometric shape—typically a paraboloid [88,105,106] or a hemisphere [34,107,108]. Other authors have assumed that the radii of curvature of the two bodies are large enough that the contact is effectively between two flat surfaces [109], or used a geometry such as a truncated cone to capture that assumption [18,110]. These latter assumptions simplify the model system significantly, but in some cases, will sacrifice fidelity to the experimental measurement. Finally, the overall size of the system must be chosen to minimize computation time while not significantly modifying the expected mechanical behavior, as discussed in Ref. [111].

For crystalline materials, the response of a nanocontact to load is dependent on the crystallographic orientation of the materials relative to the loading direction [107]. Where crystallographic information is known—for example, from experimentally measured diffraction patterns or visual analysis of a TEM image—then the model can be designed correspondingly [103,112]. Figure 5(*c*) shows a cross section of a model silicon SPM tip, where the crystallographic and loading directions are matched to those of the experimental images in Fig. 5(*a*). Some models explicitly include grain boundaries [89,113], which further improves the accuracy of the simulation for some materials. Other features that have been included in nanocontact simulations are near-surface material amorphization [103] and oxygen or hydrogen surface termination [106,107,112–114]. Finally, in cases where the tip and/or substrate contain roughness, this too may affect nanocontact behavior. Simulations can capture roughness explicitly by modifying the positions of atoms at the perimeter, either to match a known geometry or to create a desired value of a roughness parameter [89,105] such as root-mean-square (RMS) height or slope.

3.1.3 Defining Operating Conditions. Finally, once the model system is defined, the conditions under which the nanocontact exists must be established, including load and, for dynamic simulations, temperature, and speed. In a molecular statics simulation, a load is typically applied by incrementally displacing the tip and/or substrate toward each other. In molecular dynamics, load can be applied either using a displacement-based method or by directly applying a normal load to all or a subset of the atoms (often those furthest from the contact) in the tip or substrate [101]. The load is set to exactly match a corresponding experiment, if one is available for comparison. In a molecular dynamics simulation, the loading and unloading process can be modeled with a set maximum load. However, to model load accurately it requires sufficient hold time at the maximum load to allow the contact to relax to a stable configuration [35,95,103,112,115]. Also, the stiffness of an experimental cantilever/tip cannot be explicitly captured in a tip apex model, but is important in some dynamic simulations. In these cases, an additional harmonic spring is added to the model [101].

In molecular dynamics simulations, another important operating condition is temperature, which is controlled using a numerical thermostat. There are many different thermostatting schemes available. Currently, the most widely used techniques are the Langevin thermostat [116] in which a random force associated with the target temperature is added to the dynamics of atoms, and the Nosé–Hoover thermostat [117], in which a new degree-of-freedom is introduced to simulate the interaction between the atoms and a thermal bath. Often, the thermostat is applied only to the atoms away from the contact region so that the heat generated during the loading and unloading processes can be effectively dissipated, but the dynamics of the contacting atoms is not altered in the process [101]. Further, in simulations of tip movement, thermalization is typically only applied to the directions perpendicular to that movement [118]. Alternatively, one can use a Galilean invariant thermostat in the boundary region [119–121]. Either of these approaches ensures that the simulation results are not unphysically affected by the dissipation near the thermostat.

Finally, it is well known that the speeds used in molecular dynamics simulations are orders of magnitude faster than those of

typical SPM experiments. The factor that restricts simulations to fast speeds is the simulation time-step which, in order to capture the characteristic dynamics of individual atoms, is typically around 1 fs (or less for reactive potentials). The small time-step limits the maximum duration of the simulation to nanoseconds. This means that model loading and unloading speeds are typically on the order of m/s to capture a tip displacement large enough to model the entire nanocontact evolution. This speed disparity will not significantly affect results as long as the processes that occur in the contact at fast speeds are similar to those that occur at slow speeds. Accelerated simulation methods are available (as reviewed in Ref. [101]) and can be used to model phenomena that occur through a series of infrequent events, such as atomic stick–slip friction [18,110,122,123]. However, such methods may be difficult to apply to nanocontacts because contact processes may occur nearly continuously during the loading and unloading processes, and are thus not infrequent. Regardless, the key objective of these simulations is to model the nanocontact as accurately as possible, understanding the limitations of the simulation such that they can be considered when evaluating results.

3.2 Calculating Contact Area From Simulations. In atomistic simulations, contact area is determined based on information about the atoms at the interface between the two bodies. Typically, there are three stages of the process: (1) defining a criterion for atom contact; (2) identifying which or how many atoms meet that contact criterion; and then (3) converting those atoms into a measurement of area. However, there are many different ways to perform each of these steps, as illustrated in Fig. 6. The most commonly used approaches will be reviewed here.

3.2.1 Establishing a Criterion for Atomic Contact. The first step is to identify a criterion to determine which atoms are in contact. The three types of criteria typically used are force, potential energy, and distance, as shown in Fig. 6(*a*). The atoms identified using these three methods may be the same for certain simple geometries in simulations that model atomic interactions using pair potentials, but often will be different for more complex geometries and for models with many-body interactions. The force criterion is based on the concept of contact as the point at which the net interaction force on an atom from the opposite surface is repulsive. In this context, if an atom in the tip experiences a nonzero, positive force due to its interactions with the substrate, the tip atom is considered to be in contact at that time-step [62,124]. Note that other values of net force could also be used as the criterion, but a repulsive net is the most common choice. An alternative approach is to determine contact based on potential energy. The concept is based on the observation that contact atoms will have potential energies in a range that is distinguishable from that of bulk or surface, noncontact atoms [125]. Thus, once the range of energies is identified for a given system, it can be used to identify contact atoms for all subsequent simulations.

Using a distance criterion, the separation between each tip atom and the nearest substrate atom is compared to a contact cutoff distance. If the minimum distance is less than the cutoff, the atoms are said to be in contact. There are multiple ways to select a cutoff distance. The first is to use information from the interaction potential itself. Specifically, the cutoff distance can be selected to correspond to the distance at which the repulsive force becomes nonzero, the boundary of which occurs at the potential energy minimum [95,126,127], or in the case of a reactive potential, the distance at which steric repulsion or a chemical bonding event occurs [35]. This is a well-defined quantity for many potential models, but can be problematic for more complex potentials, such as metallic or three-body potentials. In such cases, the cutoff distance can be determined based on some structural feature of the materials, as opposed to using the potential function. For instance, the magnitude of the cutoff can be determined from nearest-neighbor distances, which are well defined for crystalline materials. Examples include identifying the cutoff as the second nearest-neighbor distance [128] or selecting a value slightly larger than the first nearest-neighbor distance [125]. An alternative, and one that is applicable to both crystalline and amorphous materials, is to calculate the radial distribution function (RDF), which describes the density distribution of atoms around each atom. In crystalline materials, peaks in the RDF will also correspond to nearest-neighbor distances. The location of the minimum after the first RDF peak can be used to determine a cutoff distance [115,125,129]. In all cases, the choice of cutoff distance is ultimately somewhat arbitrary because, in simulations, the interaction between atoms is a continuous quantity not a binary one.

3.2.2 Identifying Atoms in Contact. Once the criterion for contact is selected, the next step is to identify the atoms in contact (see Fig. 6(*b*)). For molecular statics simulations (or very low-temperature molecular dynamics), this process is relatively straightforward and each atom either meets the contact criterion or not. However, in molecular dynamics simulations at finite temperature, the position, force, and energy of each atom fluctuate over time. Therefore, additional decisions have to be made to determine which atoms are in contact. A detailed discussion of the different approaches and their effect on contact area is available

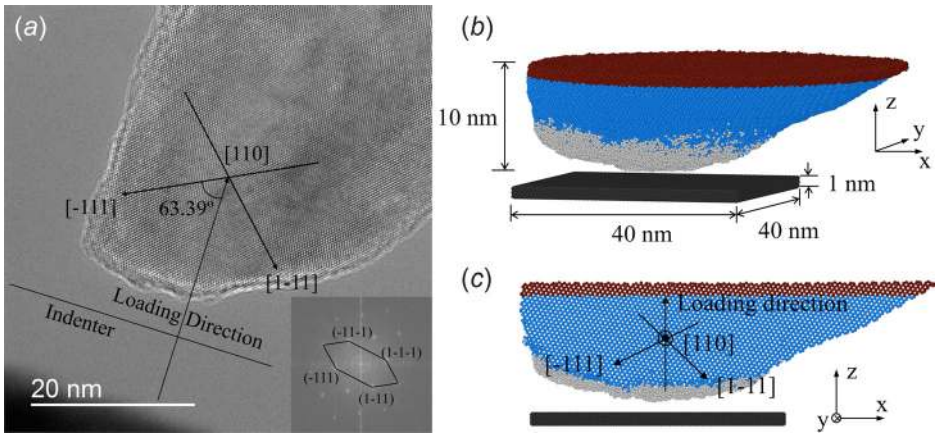

Fig. 5 (*a*) A TEM image of the tip apex immediately before contact is made, with the crystallographic orientation and loading direction identified. (*b*) An MD model was made of the lowermost 10 nm of the tip shown in (*a*) that includes both the crystalline Si and amorphous Si (a-Si) material. (*c*) A cross-sectional image of the same MD model illustrates the matching of the crystallographic orientation and loading direction. Reproduced with permission from Vishnubhotla et al. [103]. Copyright 2017 by Springer.

in Ref. [95]; they will be briefly summarized here. The simplest approach is to count the contact atoms at a certain time-step during the simulation. However, because of the thermal fluctuations inherent in the simulation, the atoms in contact (which atoms and how many) will depend on the particular time-step that is used for the calculation. Thus, some authors take a time average of the number of atoms in contact [35,36,124]. However, this method leads to additional considerations. It has been shown that, at any given time, only a small fraction of atoms carry most of the load [62,124] and so taking a time-average area over these small fractions may not be reflective of the overall contact. This effect is highlighted by counting the total number of atoms that meet a force criterion over time. As shown in Fig. 7(*a*), the number of contact atoms is larger when this calculation is performed over a longer time [62]. The various methods for identifying contact atoms from dynamic simulations can yield different results, both in terms of the number of atoms and the rate of change of that number with load. For example, it has been shown that the number of contact atoms calculated at a single instant in time from a dynamic simulation will always be proportional to load, while this is not necessarily the case for other methods of counting atoms [95].

3.2.3 Computing a Contact Area. Once the contact atoms have been identified, this information can be converted to a contact area, and multiple calculation options are available, as illustrated in Fig. 6(*c*). To calculate the nanoscopic equivalent of apparent contact area, it is common to define an in-plane shape that encloses the contact atoms and then calculate the area of that shape. Some authors use the smallest circle that encloses all (or most, e.g., 95%) of the contact atoms and then calculate analytically the area of that circle [95,108,130]. If a circular contact is assumed, another approach is to calculate the average pressure on each contact atom near the perimeter of the contact and fit the pressure versus radial position data to an analytical curve based on continuum mechanics, which can be extrapolated to identify the contact radius (see dashed line in Fig. 7(*a*)) [34,62]. Alternatively, other authors eliminate the assumption of circular contact altogether by enclosing the perimeter atoms by a convex hull (see solid line in Fig. 7(*b*)). Then the area of the resultant shape is calculated numerically [36].

The atomistic contact area (which may be closer to a concept of true contact area) can be computed by multiplying the number of contact atoms by a single-atom "area." There are two commonly used methods to determine the effective area of an individual atom. Based on the concept of the surface-atom density, the surface area of a model slab of material can be divided by the total number of atoms that comprise that surface [19,33–35,107,114]. Alternatively, by assuming a spherical atom, a circular projected area can be defined. The radius of that circle for a given atom can be calculated from the lattice constant of the material, the position of the first peak of the RDF, or the distance at the minimum energy as defined by the interaction model (these methods will typically yield the same value at 0 K) [102,115,125]. Once the effective atomic area is determined, it is multiplied by the number of contact atoms to determine the atomistic contact area.

4 Different Theories to Describe Contact Area and Their Potential Applicability at the Nanoscale

There are three competing theories that are commonly used to describe the behavior of nanocontacts (Fig. 8):

- *Single-contact continuum mechanics:* Nanocontacts can be described using continuum mechanics models of smooth shapes (e.g., spheres) with a single continuous contact.
- *Multiple-contact continuum mechanics:* Because of surface roughness, nanocontacts can be described by the collective behavior of a group of smaller subcontacts, where the mechanical response can be calculated using continuum mechanics. These models are typically based either on the geometry of multiple identical asperities of varying height, or on multiscale descriptions of surface roughness.
- *Atomistic accounting:* Nanocontacts can be described as a collection of single-atom junctions, which may not behave according to continuum theory.

Fundamentally, these three theories (described in more detail in Secs. 4.1–4.3) embody three very different pictures of what it means to be in contact at the nanoscale.

4.1 Single-Contact Continuum Mechanics

4.1.1 Single-Asperity Contact Mechanics. One approach to describe nanocontacts is to use the well-established framework of contact mechanics. That is, to assume well-defined smooth geometric shapes of the bodies in contact, and the applicability of continuum mechanics. By defining contact as the point of zero gap, the behavior can be modeled under various conditions. The general prediction of models based on this concept is that contact area increases sublinearly with load, as illustrated by the example in Fig. 8(*a*).

4.1.1.1 Spherical contact mechanics models. Continuum mechanics has been applied to model contact between adhesive and nonadhesive spheres. This topic has been thoroughly reviewed elsewhere [50,132–134], so only the key results will be presented here. In 1885, Heinrich Hertz used elasticity theory to describe the compression of elastic, nonadhesive spheres [135]. He showed that their area of contact is given by [50]

$$A_{\text{Hertz}} = \pi\left(\frac{3F_{\text{app}}R}{4E^*}\right)^{2/3} \tag{12}$$

where F_{app} is the load, R is the effective radius of the contacting bodies, $R = ((1/R_1) + (1/R_2))^{-1}$, and E^* is the effective elastic modulus. An adhesive version of the same solution was presented by Derjaguin–Müller–Toporov (DMT) [136], where Eq. (12) is still used—but F_{app} is replaced by $F_{\text{total}} = F_{\text{app}} + F_{\text{pull-off}}$. The pull-off force can be directly measured, or if the work of adhesion W_{adh} is known, then $F_{\text{total}} = F_{\text{app}} + 2\pi RW_{\text{adh}}$. A conflicting description of adhesive spheres, the Johnson–Kendall–Roberts (JKR) model [137], was developed based on fracture mechanics and gave the following contact area:

$$A_{\text{JKR}} = \pi\left\{\frac{3R}{4E^*}\left[F_{\text{app}} + 3W_{\text{adh}}\pi R + \sqrt{6W_{\text{adh}}\pi RF_{\text{app}} + (3W_{\text{adh}}\pi R)^2}\right]\right\}^{2/3} \tag{13}$$

where F_{adh} in this model is determined as $(3/2)\pi RW_{\text{adh}}$. Tabor [138] described the conflicting JKR and DMT models as two limiting cases of strong short-range interactions and weak long-range interactions, respectively. He described a transition parameter to determine whether a particular situation obeyed one of these limiting cases or fell in an intermediate regime

$$\mu_T = \left(\frac{RW_{\text{adh}}^2}{E^{*2}z_0^3}\right)^{1/3} \tag{14}$$

where z_0 is the equilibrium separation distance. Maugis [133] later used a "Dugdale" interaction potential to quantitatively demonstrate what Tabor had described, and to mathematically determine the behavior in the intermediate region. In Maugis' formulation, the equilibrium distance is replaced by the range of adhesion, which is typically similar in magnitude to the equilibrium separation distance. The contact area in the intermediate region can be

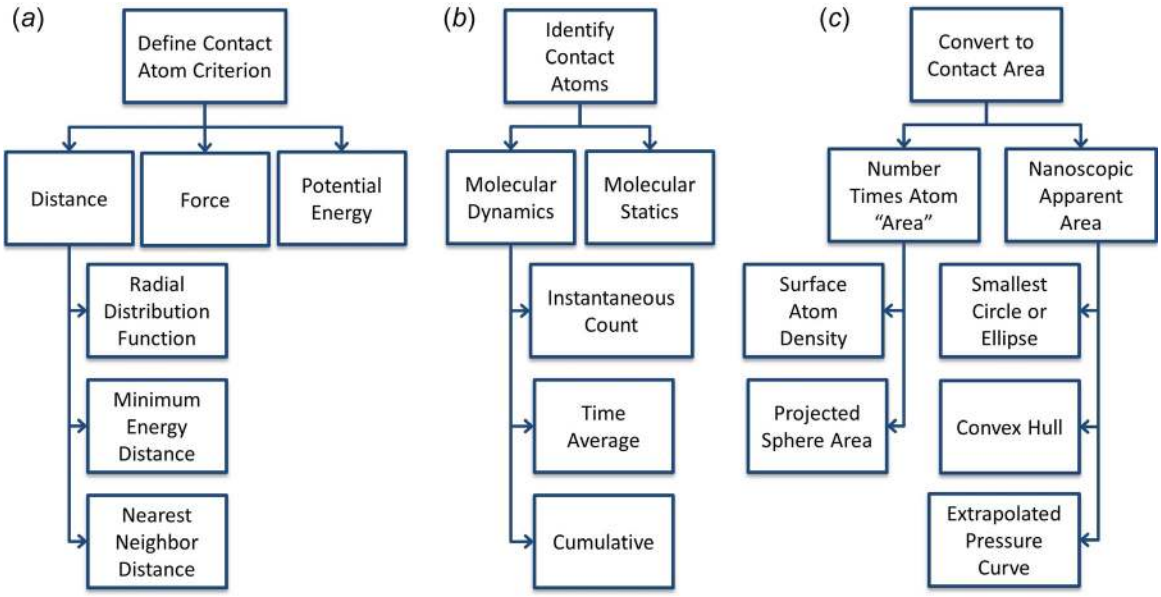

Fig. 6 Various methods are used to calculate contact area from atomistic simulations. The three key steps are: (*a*) define contact criterion, (*b*) identify contact atoms, and (*c*) calculate contact area.

numerically calculated using the Carpick–Ogletree–Salmeron method [139].

4.1.1.2 Single-asperity models for more complex cases. The above elastic spherical models yield equations for contact parameters and represent a good starting point for analysis. For these reasons, they are widely used in scientific investigations and technological applications. However, they rely on significant assumptions, namely that: (i) the materials are homogeneous, isotropic, and linear elastic; (ii) the global shape of both bodies is spherical (or, more accurately, paraboloidal); (iii) the local shape of both bodies is perfectly smooth; (iv) the contact size is small relative to the sphere radius; (v) deformations are small compared to the sphere radius; and (vi) that the surfaces are frictionless. Important extensions to these solutions have been proposed to incorporate aspherical shapes [140,141], anisotropic material properties [142–144], thin-film coatings [145–147], and plasticity [51,148,149].

4.1.1.3 Assumptions of single-asperity models and potential flaws at the nanoscale. The advantage of these solutions is that they yield analytical or numerical equations for computing contact parameters such as contact size. However, all of these models rely on the assumption that the geometries of the bodies are those of smooth, well-defined geometric shapes and that contact occurs in a single region. Further, they all assume that both bodies are continuous, whereas the scale of nanocontacts is often sufficiently small that atomic-scale details become relevant (see Fig. 2). Further, most of these models rely on small-strain approximations where the stresses are low relative to failure stresses and the contact radius is small relative to the radius of either body. For nanoscale contacts, the small radius of curvature can lead to the

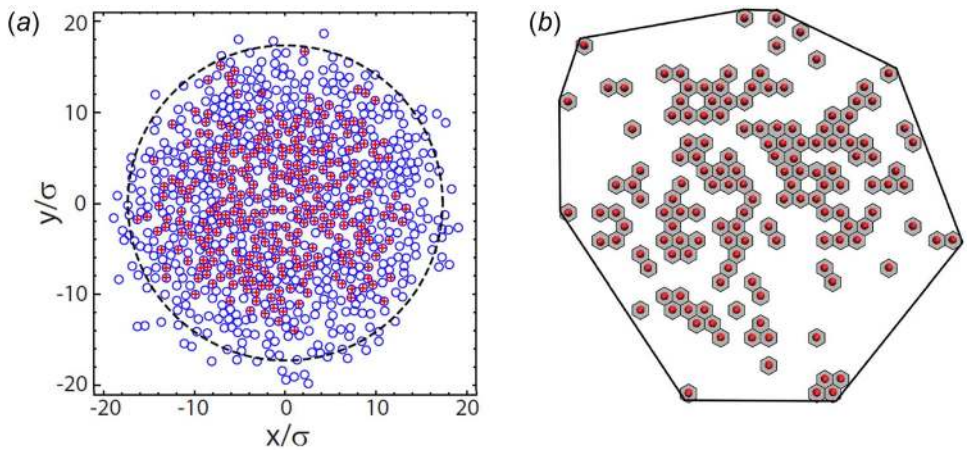

Fig. 7 (*a*) For an amorphous contact, a significantly different number of atoms are identified as being in contact when measured over short time interval (red plusses) as compared to a long one (open blue circles). The large dashed circle shows the radius determined from the pressure distribution obtained from the long-time interval calculation. Image reproduced with permission from Cheng et al. [62]. Copyright 2010 by American Physical Society. (*b*) Some authors define an atomistic contact area using the contacting atoms, and an apparent contact area as the convex hull that contains all such atoms. Image reproduced with permission from Mo et al. [36]. Copyright 2009 by Nature Publishing Group. (A color version of this figure is available online.)

violation of both of these assumptions, sometimes under the action of adhesion alone.

4.1.2 Experimental Support for the Application of Single-Contact Continuum Mechanics to Nanocontacts. The primary experimental evidence to support the application of single-asperity models to nanocontacts comes from extremely well-controlled contacts made using SPM, including those in ultra-high vacuum. For instance, for a carbon-based spherical tip sliding on a wide variety of surfaces, the friction versus normal load curve could be extremely well fit using spherical contact mechanics under the assumption that the friction is proportional to the true contact area [150,151]. Also, spherical models have been used to describe the friction of a Pt-coated tip in contact with muscovite mica [59]. For ohmic (Pt/graphite) and semiconducting contacts (doped-silicon/NbSe2) [45], the load dependence of contact conductance was shown to obey a Maugis–Dugdale model and to correlate well with estimates of contact area computed from the contact-stiffness approach (Eq. (6)). A study of tungsten carbide tips on hydrogen-terminated diamond [43,44] showed that the load dependence of contact resistance and friction could be well correlated to each other and to the DMT model. Similar trends were reproduced using silicon nitride tips on self-assembled monolayers [152]. Additional indirect support of these models is provided by a large number of papers (for example, Refs. [88] and [152]) that *assume* a continuum contact model to apply and obtain an accurate fit to experimental data with reasonable fitting parameters.

However, a cautionary note is provided by the authors of some of the aforementioned studies: it is clear that sliding wear [45] and contamination [45,47] cause real-time changes in tip shape that cannot generally be accounted for in SPM experiments. Lantz and coworkers even concluded that contact resistance should be used "to verify the variation in A with load, [but] cannot presently be applied with confidence to find the absolute values of A" [45]. They point to several difficulties of the technique, including (a) uncertainties in the electron mean free path, (b) uncertainties in the shape of the tip, (c) the effect of plastic deformation, and (d) deviations from ideal behavior for nonohmic contacts or those with contamination or oxides—and some of these factors can evolve over the course of a single experiment.

4.1.3 Simulation Support for the Application of Single-Contact Continuum Mechanics to Nanocontacts. The discrete nature of atomistic simulations means that they violate many of the assumptions of contact mechanics theories. However, there is still some support for a single-asperity continuum mechanics view of contact from such simulations. For example, simulations of contact on alkylsilane self-assembled monolayers [108] yielded contact area calculations qualitatively and quantitatively consistent with that predicted by a thin-coating contact mechanics model [146]. Other simulations indicated that continuum mechanics theories could be applicable, but only under specific conditions. For example, it was suggested that deviations from continuum theory are due to local plasticity during the indentation process, and that atomistic simulation results and continuum theories may match at very small indentation depths (less than ~3 Å) while the material response is still elastic [102]. It has also been reported that the agreement between atomistic simulations and continuum mechanics models depends on how contact area is calculated from the simulation. For example, one study showed that calculating the contact radius from a simulation using the second moment of the pressure distribution yielded results closer to continuum mechanics prediction [62]. Finally, some authors assume that the form of the continuum equations is correct and suitable for describing contacts in atomistic simulation, but that the parameters in those equations should be modified to capture the atomic-scale features of the two bodies and their interactions. For example, it was shown that atomistic simulation data are consistent with predictions from the Maugis–Dugdale theory if the work of adhesion is treated as a fit parameter [95]. These findings suggest empirically that, at least in some cases, the continuum equations can be usefully applied at small scales.

4.2 Multiple-Contact Continuum Mechanics. Another approach to describe nanocontacts is to use multi-asperity continuum models that have been established for planar surfaces containing roughness. These account for surface roughness using simplifying assumptions, and then apply continuum mechanics. Contact is still defined as the point of zero separation between the bodies, but the contact is no longer assumed to be continuous. Significantly, while single-asperity contact models predict a sublinear dependence of contact area on load, multi-asperity models predict a linear relationship, shown in the example in Fig. 8(*b*).

4.2.1 Rough-Surface Continuum Contact Models. Bowden and Tabor recognized in their classic work of metal friction [31] the important role that surface roughness plays in contact properties, including that the *true* area of contact (described in Sec. 1.3) is often patchy and is orders of magnitude smaller than the apparent value. Many different mechanics models have been proposed to describe contact between nominally planar surfaces that contain roughness. This topic has been reviewed elsewhere [153–156] and only the most salient points are presented here. In these models, the random and complicated roughness of a real surface is replaced by a simpler description of the surface. Then, the mechanics of the contact can be computed analytically or numerically, and contact properties (such as contact area) can be calculated. These models can be grouped according to the character of the modeled roughness: with *single-scale models* assuming that roughness can be described using an array of noninteracting features of a single size; and *multiscale models* assuming that real roughness is most accurately described by a hierarchy, where larger features have smaller features superimposed on top of them, which in turn have even smaller features superimposed onto them, and so on (as first suggested in Ref. [157]).

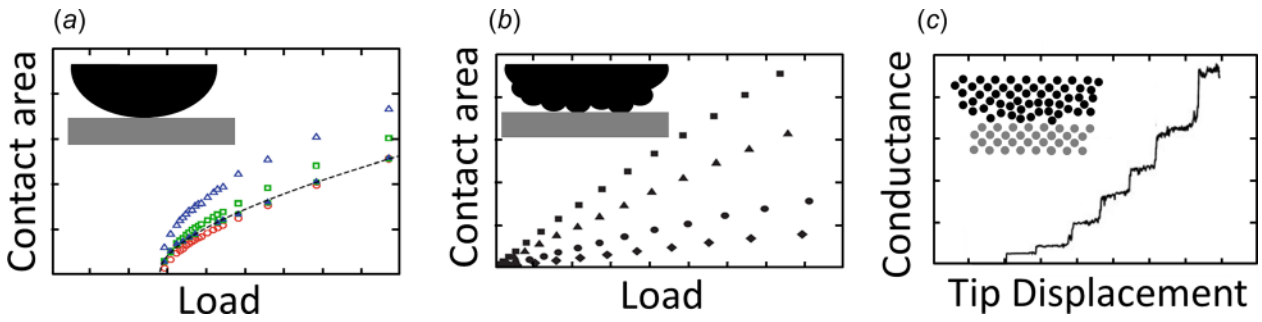

Fig. 8 Competing theories predict different behavior: (*a*) single-contact continuum mechanics, (*b*) multiple-contact continuum mechanics, and (*c*) atomistic accounting. The graphs in (*a*), (*b*), and (*c*) were created using data from Refs. [95], [35], and [131], respectively.

4.2.1.1 Single-scale models of roughness. The most influential early analytical theory for contact between rough surfaces is the 1966 model of Greenwood and Williamson [22], which represented a rough contact as a large number of noninteracting spherical asperities with identical radii and a Gaussian distribution of heights. Hertzian contact mechanics was applied to each asperity individually. Over the subsequent decades, this model was extended to include different distributions of asperity heights [158–161] and asperity radii [162,163], as well as contributions from plasticity [25,26] and adhesion [23,24]. A key outcome of these models is that the most significant parameter for contact area is the amplitude of height fluctuations, e.g., the root-mean-square height. Greenwood–Williamson-type models are simpler to implement than multiscale approaches and are able to reproduce some trends in large-scale experimental behavior. However, these models do not reflect the geometry of many rough surfaces (which is very commonly multiscale, e.g., see Ref. [164]) and account neither for mechanical interactions between individual asperities nor for spatial correlations in roughness.

4.2.1.2 Multiscale models of roughness. Later roughness models [60,165–169] incorporated the multiscale nature of surface roughness by describing surface topography as a hierarchical set of features. These models account for interactions between contact points and are more representative of the measured topography of real surfaces [170,171]. Some of these models take advantage of the fact that a wide variety of real surfaces display fractal-like self-affine scaling [164,172–175]. Mathematically, this means that the amplitude of (Gaussian) height fluctuations δh between two points on the surface separated by a distance l scales as $\delta h \propto l^H$ [164,172,174], where H is a constant between 0 and 1 [176] that is related to the fractal dimension [176] of the surface. This description has been shown [177] to represent the topography of a wide variety of surfaces, including metals [178–180] and glasses [181,182].

Recently, Persson [28,183] presented an analytical model for the elastic contact of random, self-affine surfaces. This theory can be solved to obtain contact area, and predicts proportionality with load over a large range of loads. This result is in good agreement with experimental findings [184] and numerical calculations [185], and is consistent with Amontons' widely observed friction law [173,186]. Persson's theory has been subsequently extended for adhesive contact [20,187–190]. In contrast to Greenwood–Williamson-type models, Persson's model (and its extensions) identifies the amplitude of fluctuations of local slope, the RMS slope, as the parameter controlling contact area [185,191–192]. While the *RMS height* depends primarily on the longest-wavelength contributions to roughness, the *RMS slope* depends mostly on the shortest-wavelength contributions [177].

4.2.1.3 Assumptions of these theories and potential flaws at the nanoscale. Similar to single-contact models, these multicontact models rely on continuum mechanics, which may not be applicable down to the atomic scale. Additionally, these models treat the surfaces as continuous such that quantities such as RMS slope are straightforwardly defined from the local derivatives of the continuous surface topography. By contrast, real surfaces have atomic structure at the surface, and the atomic interpretation of quantities such as surface slope is not entirely clear. An additional challenge of the application of large-scale roughness models to the nanoscale is that these models assume a separation of length scales between the size scale of the roughness and the size of the bodies in contact. Greenwood–Williamson-type models assume a stochastic distribution of heights of the interacting asperities, which implies sampling over a large area. Likewise, multiscale models assume contributions over a large range of spatial frequencies. In both cases, the small geometry of a nanocontact could lead to significant finite-size effects, [193] because the actual contact is sampling roughness over a very limited scale.

4.2.2 Experimental Support for the Application of Multicontact Continuum Mechanics to Nanocontacts. Few experimental reports have directly applied these rough-contact elastic models to nanoscale tips. Instead, the experimental evidence for a multicontact description of nanocontacts comes primarily from studies where the topography of the tip has been characterized accurately and then experimental measurements were performed and characterized in light of the topographic information. For example, using contact stiffness measurements of SPM probes that had been pre-characterized in the scanning electron microscope, it was shown that continuum contact mechanics *could* be fit to the measured data, but the resultant fitting parameters did not agree with measured values. The tip radii determined from the mechanics fits were significantly smaller than the values determined from imaging [39]. The authors interpreted this finding, along with the measured linearity of contact stiffness with load, as consistent with the tip not engaging the surface as a single sphere, but rather as a series of subscale protrusions. Similarly, using lateral stiffness measurements of SPM probes with unknown radii [46], the single-sphere contact mechanics approach yielded an unphysically small contact radius.

In other SPM investigations, adhesion was measured between a sharp tip and a rough substrate [194–197]. The experimental data were accurately fit in all cases by assuming a simplified multi-asperity contact and then computing the resulting van der Waals contribution to adhesion. Separate adhesion tests performed with in situ characterization of tip geometry were also modeled using multi-asperity descriptions of nanocontacts. For tips coated with diamond-like carbon and ultrananocrystalline diamond in contact with a diamond substrate [89], the decrease in adhesion with increasing roughness could be accurately fit using a simplified roughness model, based on a single-scale van der Waals integration. A separate study of silicon tips with a native oxide in contact with diamond [90,91] accounted for the arbitrary roughness of the tip and integrated an interaction potential over the measured geometry. This approach yielded more accurate adhesion parameters than the application of a spherical contact model. A similar approach was also applied to a hard/soft contact with an ultrananocrystalline diamond tip in contact with a polymethylmethacrylate surface [198]. In all of these investigations, the experimental behavior of a rough nanoscale contact was modeled as interacting via multiple smaller contacts.

4.2.3 Simulation Support for the Application of Multiple-Contact Continuum Mechanics to Nanocontacts. Some simulations of single asperities have been shown to exhibit rough contact model behavior, i.e., a linear increase of contact area with load. While roughness classically refers to asperities on a surface, for single asperity contact, roughness might be interpreted as atomic-scale features on the surface of the asperity. In this context, atomistic simulation data have been used to suggest an adhesion-induced transition between continuum-like and non-continuum-like behavior for nanocontacts [35,36]. The conclusion was that nanocontacts can be expected to exhibit continuum-like area–load proportionality if the surfaces are sufficiently rough at the atomic scale. However, the contact area calculation method used in those papers was based on a time-averaged number of contact atoms, which could also explain the observed linear relationship [95]. In addition, recent simulations of rough spheres [199] showed that a linear relationship between load and contact area can only be expected when the surface roughness is much smaller than the radius of the sphere. For the smaller radii that are characteristic of an SPM tip, the linear region was not observed in that investigation, suggesting a minimum size for the applicability of rough surface contact theories. It is also notable that a linearly increasing contact area with load has been observed in atomistic simulations of nominally flat surfaces with nanoscale roughness [60,200,201] or with multiple nanoparticles [202], as well as in non-atomistic numerical simulations of nominally flat, rough surfaces [60,165,203–205].

In summary, while there is experimental and simulation evidence that nanocontacts can by patchy and discontinuous, there is not yet clear evidence that the well-established planar roughness models can be applied at the nanoscale.

4.3 Atomistic Accounting. The last of the three theories is based on the premise that nanocontacts should not be described by continuum mechanics models at all since the assumptions that underlie those models do not apply at the atomic scale. This is supported by examples where contact area varies with load in a way that cannot be described by any continuum model, as in Fig. 8(*c*). Instead, the complete interatomic interactions must be considered.

4.3.1 An Atomic-Scale Description of Contact. Early evidence for deviation from continuum contact mechanics theory was observed in investigations using mechanically controllable break junctions (Sec. 2) with the formation of an atomic neck in soft metals and with quantized drops in conductance and force during unloading. Such behavior is certainly not predicted by classical contact mechanics models and suggests that an entirely different description of contact is required at the nanoscale. It is instead proposed that nanocontacts are comprised of a collection of single-atomic junctions and that the behavior of the whole contact simply reflects the collective behavior of the individual junctions. In this view, the very concept of contact area is secondary to a complete description of the forces and transport between atoms across the interface. The challenge with the atomistic accounting is that, in the absence of mechanics models, there is no single agreed-upon method or parameter to generalize behavior. The implication is then that each nanocontact is unique and will depend on the details of the materials, geometry, type of bonding at the interface, etc. This makes atomistic accounting difficult to apply outside of the context of a fully atomistic simulation or a very limited set of experimental conditions.

4.3.2 Experimental Support for Atomistic Accounting in Nanocontacts. Experimental support for noncontinuum nanocontact behavior primarily comes from measurements of spontaneously welding metals like gold, where the two bodies form an almost liquid-like bridge across the contact [37,206]. In these cases, the original contact interface is neither well defined nor relevant—rather, the properties of the contact are determined by the behavior of the bridge. As mentioned, break-junction investigations have demonstrated quantized changes in conduction (e.g., see Ref. [131]), representing changes in the available quantum modes as additional atomic chains are formed or severed. This mechanism has been verified using in situ TEM studies [81–85]. These contacts are not typically described in terms of their area of contact, but rather as the number of atoms in contact. And while continuum parameters such as yield strength can be computed for such atomic junctions, the results are most accurately described with atomistic concepts, such as surface diffusion and bond formation/breakage. Simultaneous measurements of conductance and load during approach/separation [131,207] show that, while conductance and mechanical stiffness (calculated using a continuum equation) often exhibit discontinuities at the same time, there are additional variations in stiffness that cannot be correlated with changes in conductance. This indicates that a simple application of continuum mechanics models with the area of contact directly proportional to number of atoms may not be accurate. As additional support for an atomistic picture, the aforementioned measurements of thermal contact resistance [38] have been accurately fit using a model of quantized thermal conductance, where the transport of the entire contact was proportional to the number of atoms in contact.

4.3.3 Simulation Support for Atomistic Accounting in Nanocontacts. Early simulation-based evidence of nanocontact behavior that deviates from continuum theory came from soft metals and the observation of a neck at the contact, similar to the break junction experiments. These simulations showed that unloading occurs through elongation of an atomically thin neck. This elongation is characterized by periods of elastic deformation separated by abrupt structural atomic rearrangements in which the length and cross section of the contact change sharply [208,209]. Since those initial studies, many other simulations of soft metals have demonstrated similar behavior, where the formation and separation of a neck of material is characterized by discrete atomic-scale events [210–213]. These discrete events also correspond to abrupt changes in the contact force. Further investigations captured the simultaneous jumps in force and conductance during unloading [130,214,215], which had been observed experimentally. Additionally, separate simulations of the friction between gold interfaces [19] suggested that the bulk friction depends fundamentally on the interatomic interactions, more so than any continuum-like contact area.

There is also evidence for noncontinuum behavior from atomistic simulations of other materials (besides soft metals). Simulations of small-radii diamond indenters showed that the contact area calculated from the simulation was consistently larger than that predicted by continuum contact mechanics models [102,107,113]. The difference between atomistic and continuum contact areas is typically attributed to the fact that the simulations violate the assumptions on which the continuum contact theories are based. For example, continuum theories assume that the geometries of the contacting bodies can be completely described by the radius of the body. However, simulations of hemispheres having the same effective radius but different atomic-scale features yielded very different (2–4 times) values of the work of adhesion and contact area [33,34]. In this case, the primary source of the difference was identified as atomic corrugation, causing deviations from an ideal analytical shape and associated concerns about commensurability of the two contacting surfaces. It has also been found that the majority of a normal load applied on a tip in an atomistic simulation is supported by a relatively small number of atoms in the interface. For example, in a simulation where 1320 atoms were identified as being in contact based on the nonzero force criterion, 96% of the overall load was supported by just 32 atoms [124]. This behavior is not predicted by continuum mechanics model and supports the argument that atomic accounting may be necessary to fully describe some features of nanocontacts.

5 Summary and Outlook: Implications for the Continued Investigation of Nanocontacts

Taken together, this extensive body of research not only represents substantial progress in our understanding of contact at the nanoscale, but also suggests that significant gaps remain.

There are concrete technological and scientific benefits to achieving a predictive understanding of contact area at the nanoscale. First, this understanding would guide optimization of performance in real-world applications (such as scanning probe microscopy, nanodevices, and nanomanufacturing) where the size of the contact determines resolution, accuracy, and reliability of the technique. Second, there are unanswered scientific questions about the physical processes that underlie friction, adhesion, wear, and interfacial transport—all of which would benefit from independent knowledge of the size and shape of contact under a certain set of conditions. Third, there are many cases where correlations are observed between contact properties (such as between thermal or electrical contact resistance and lateral stiffness or frictional forces). If the size and character of the contact is the underlying factor that controls these parameters, then an understanding of contact area would greatly enhance the ability to predict multiple properties based on measurement or calculation of just one. And finally, while there are cases where atomic-scale detail is known and properties can be calculated atomistically (such that the concept of contact area is not required), there are far more cases where atomistic simulations are impractical or cannot

be used to predict a particular property of interest. In these cases, a more coarse-grained concept such as contact area will enable prediction of properties, and generalizability of measured results.

However, gaining this understanding of the nanoscale contact area is nontrivial. Experimentally, the contact area is often computed from measured properties, but this relies on significant assumptions about the character of the contact and models to describe it—many of which are unproven at the nanoscale. From a simulation perspective, the atomic-scale behavior can be determined, but quantifying contact area is ambiguous. The calculation requires: (1) selection of a criterion for determining which atoms are in contact, (2) a method for identifying which atoms meet this criterion, and (3) conversion from the number of atoms in contact to the area of contact. In both experiments and simulations, the choices made during analysis of contact area can have significant effects on the measured result.

The above discussion demonstrates that no single technique or measurement will suffice for accurately determining contact area at the nanoscale. This implies that, for any report of contact area obtained using a single technique, the methods used and assumptions made should be fully described so that the value can be interpreted correspondingly. Alternatively, the most promising approaches may include the use of multiple independent techniques simultaneously. As an experimental example, many or all of the measurements described in Sec. 2 can be combined. Scanning probe microscopy is becoming sufficiently versatile and sophisticated such that simultaneous measurements can be made of contact resistance, normal contact stiffness, lateral contact stiffness, sliding friction, and topography to combine many indirect measurements at once. The absolute values of contact area measured with each approach can be quantitatively compared, including as a function of applied load—and the correlations between them (or lack thereof) can be used to evaluate various models under different conditions. Further, with the growing use of in situ apparatuses, indirect methods for evaluating contact area can be combined with direct methods—to interrogate assumptions about materials, geometries, and amount of deformation. Multiple methods can be combined in simulation studies as well. For instance, for a single simulation, multiple different contact criteria can be used, and the results of each can be evaluated using various methods of determining contact area (Sec. 3). All of these can be compared against the computed values of physically measurable quantities, such as normal and lateral contact stiffness, in order to evaluate connections between them. Finally, the most conclusive strategy may be the combination of experiments and simulations that are optimally matched in terms of geometry, materials, loading conditions, and environment. This will enable the simulations to be validated by comparison to the experiments; then the simulations and experiments can be used together to provide a complete picture of the nanocontact of interest. The goal is the establishment of a connection between atomic-scale interactions and experimentally measurable quantities, which is complete with a consistent picture of contact area. This type of combined investigation has the potential to significantly enhance our understanding of contact.

A challenge that stands in the way of unification among atomistic simulations, continuum models, and real-world experiments is the definition of contact. As has been pointed out in this review, the conventional definition of contact in a continuum sense is the point of zero gap, while typical criteria in atomistic simulations would be either zero force between atoms or a state of net repulsion. These criteria are in conflict, as demonstrated by a classical JKR contact. In this, the contact contains an inner circle where the normal stress is compressive and an outer concentric annulus where the normal stress is tensile. In the continuum picture, both regions are considered to be in contact; yet by most atomistic criteria, the outer ring would not be counted as contact. This is an example where a continuum model and an atomistic simulation might be identical in terms of the overall configuration of deformations and stresses, yet could result in different calculated values for contact area. These differences are not irreconcilable. For instance, the continuum definition of contact could be redefined using a zero-load or a repulsive-interaction criterion—or the atomistic criterion could be adjusted to include a larger separation and/or a more negative load. In either case, these definitions must be standardized and co-validated, both between experiment and simulation, and against some experimentally measurable property. Only then can a consistent picture of contact area emerge.

As discussed in Sec. 4, there are different theories available to describe nanoscale contact, most of which have been validated over limited regimes and sometimes using just one experimental or simulation-based approach. It is almost certain that all three of the theories are correct and simply represent different limits of behavior. To comprehensively interrogate the various contact theories, it will be necessary to perform multimodal contact measurements and simulations. These will need to be performed on a wide variety of systems, which vary significantly in terms of materials, shape, and size of the bodies, roughness of the surfaces, and conditions of load, speed, and environment. Further, the quantitative comparison of contact area as measured using different approaches will enable specific predictions of each theory to be confirmed or refuted. Ultimately, continued research in this field will guide the delineation of boundaries to determine concretely which theories apply over which ranges of conditions.

In conclusion, this review has shown that nanocontacts exhibit a complex set of behaviors as they form, evolve, and separate. However, the fact that they are buried between two surfaces also means that they present a significant challenge to the research community. This challenge has been pursued by researchers from a range of disciplines, including physicists, chemists, mechanical engineers, and materials scientists. Using a variety of different methods and approaches, researchers have slowly begun to uncover the science within the buried interface. Significant challenges and opportunities remain, many of which will need to be tackled using a complementary set of experimental and simulation tools to interrogate contact theories. The ultimate goal of these efforts is to fundamentally understand what it means to be in contact at the nanoscale.

Acknowledgment

The authors thank Dr. Lars Pastewka for review and helpful feedback on the manuscript.

Funding Data

- Air Force Office of Scientific Research (Grant No. FA9550-15-1-0256).
- National Science Foundation (Grant Nos. CMMI-1536800 and CMMI-1537613).

References

[1] Hurley, D. C., Kopycinska-Müller, M., Kos, A. B., and Geiss, R. H., 2005, "Nanoscale Elastic-Property Measurements and Mapping Using Atomic Force Acoustic Microscopy Methods," Meas. Sci. Technol., **16**(11), pp. 2167–2172.

[2] Hurley, D. C., Shen, K., Jennett, N. M., and Turner, J. A., 2003, "Atomic Force Acoustic Microscopy Methods to Determine Thin-Film Elastic Properties," J. Appl. Phys., **94**(4), pp. 2347–2349.

[3] Born, A., and Wiesendanger, R., 1998, "Scanning Capacitance Microscope as a Tool for the Characterization of Integrated Circuits," Appl. Phys. A, **66**(7), pp. S421–S426.

[4] Bussmann, E., and Williams, C. C., 2004, "Sub-10 nm Lateral Spatial Resolution in Scanning Capacitance Microscopy Achieved With Solid Platinum Probes," Rev. Sci. Instrum., **75**(2), pp. 422–425.

[5] Kelley, T. W., Granstrom, E. L., and Frisbie, C. D., 1999, "Conducting Probe Atomic Force Microscopy: A Characterization Tool for Molecular Electronics," Adv. Mater., **11**(3), pp. 261–264.

[6] Majumdar, A., 1999, "Scanning Thermal Microscopy," Annu. Rev. Mater. Sci., **29**(1), pp. 505–585.

[7] Jesse, S., Kumar, A., Arruda, T. M., Kim, Y., Kalinin, S. V., and Ciucci, F., 2012, "Electrochemical Strain Microscopy: Probing Ionic and Electrochemical Phenomena in Solids at the Nanometer Level," MRS Bull., **37**(7), pp. 651–658.
[8] Kalinin, S., and Bonnell, D., 2002, "Imaging Mechanism of Piezoresponse Force Microscopy of Ferroelectric Surfaces," Phys. Rev. B, **65**(12), p. 125408.
[9] Denning, D., Guyonnet, J., and Rodriguez, B. J., 2016, "Applications of Piezoresponse Force Microscopy in Materials Research: From Inorganic Ferroelectrics to Biopiezoelectrics and Beyond," Int. Mater. Rev., **61**(1), pp. 46–70.
[10] Garcia, R., Knoll, A. W., and Riedo, E., 2014, "Advanced Scanning Probe Lithography," Nat. Nanotechnol., **9**(8), pp. 577–587.
[11] Masubuchi, S., Ono, M., Yoshida, K., Hirakawa, K., and Machida, T., 2009, "Fabrication of Graphene Nanoribbon by Local Anodic Oxidation Lithography Using Atomic Force Microscope," Appl. Phys. Lett., **94**(8), p. 082107.
[12] Cen, C., Thiel, S., Hammerl, G., and Schneider, C. W., 2008, "Nanoscale Control of an Interfacial Metal–Insulator Transition at Room Temperature," Nat. Mater., **7**(4), pp. 298–302.
[13] Pires, D., Hedrick, J. L., De Silva, A., Frommer, J., Gotsmann, B., Wolf, H., Despont, M., Duerig, U., and Knoll, A. W., 2010, "Nanoscale Three-Dimensional Patterning of Molecular Resists by Scanning Probes," Science, **328**(5979), pp. 732–735.
[14] Chou, S. Y., Krauss, P. R., and Renstrom, P. J., 1995, "Imprint of Sub-25 nm Vias and Trenches in Polymers," Appl. Phys. Lett., **67**(21), pp. 3114–3116.
[15] Kim, T. H., Cho, K. S., Lee, E. K., Lee, S. J., Chae, J., and Kim, J. W., 2011, "Full-Colour Quantum Dot Displays Fabricated by Transfer Printing," Nature, **5**(3), pp. 176–182.
[16] Rebeiz, G. M., and Muldavin, J. B., 2001, "RF MEMS Switches and Switch Circuits," Microwave Mag., **2**(4), pp. 59–71.
[17] Loh, O. Y., and Espinosa, H. D., 2012, "Nanoelectromechanical Contact Switches," Nat. Nanotechnol., **7**(5), pp. 283–295.
[18] Li, Q., Dong, Y., Perez, D., Martini, A., and Carpick, R. W., 2011, "Speed Dependence of Atomic Stick-Slip Friction in Optimally Matched Experiments and Molecular Dynamics Simulations," Phys. Rev. Lett., **106**(12), p. 126101.
[19] Gao, J., Luedtke, W. D., Gourdon, D., Ruths, M., Israelachvili, J. N., and Landman, U., 2004, "Frictional Forces and Amontons' Law: From the Molecular to the Macroscopic Scale," J. Phys. Chem. B, **108**(11), pp. 3410–3425.
[20] Persson, B. N. J., Sivebaek, I. M., Samoilov, V. N., Zhao, K., Volokitin, A. I., and Zhang, Z., 2008, "On the Origin of Amonton's Friction Law," J. Phys.: Condens. Matter, **20**(39), p. 395006.
[21] Müser, M. H., Wenning, L., and Robbins, M. O., 2001, "Simple Microscopic Theory of Amontons's Laws for Static Friction," Phys. Rev. Lett., **86**(7), pp. 1295–1298.
[22] Greenwood, J., and Williamson, J., 1966, "Contact of Nominally Flat Surfaces," Proc. R. Soc. A, **295**(1442), pp. 300–319.
[23] Fuller, K., and Tabor, D., 1975, "Effect of Surface-Roughness on Adhesion of Elastic Solids," Proc. R. Soc. A, **345**(1642), pp. 327–342.
[24] Maugis, D., 1996, "On the Contact and Adhesion of Rough Surfaces," J. Adhes. Sci. Technol., **10**(2), pp. 161–175.
[25] Kogut, L., and Etsion, I., 2003, "A Finite Element Based Elastic-Plastic Model for the Contact of Rough Surfaces," Tribol. Trans., **46**(3), pp. 383–390.
[26] Chang, W., Etsion, I., and Bogy, D., 1987, "An Elastic-Plastic Model for the Contact of Rough Surfaces," ASME J. Tribol., **109**(2), pp. 257–263.
[27] Persson, B. N. J., 2006, "Contact Mechanics for Randomly Rough Surfaces," Surf. Sci. Rep., **61**(4), pp. 201–227.
[28] Persson, B. N. J., 2001, "Elastoplastic Contact Between Randomly Rough Surfaces," Phys. Rev. Lett., **87**(11), p. 116101.
[29] Majumdar, A., and Tien, C. L., 1990, "Fractal Characterization and Simulation of Rough Surfaces," Wear, **136**(2), pp. 313–327.
[30] Ciavarella, M., Delfine, V., and Demelio, G., 2006, "A 'Re-Vitalized' Greenwood and Williamson Model of Elastic Contact Between Fractal Surfaces," J. Mech. Phys. Solids, **54**(12), pp. 2569–2591.
[31] Bowden, F. P., and Tabor, D., 1939, "The Area of Contact Between Stationary and Between Moving Surfaces," Proc. R. Soc. A, **169**(938), pp. 391–413.
[32] Archard, J. F., 1953, "Contact and Rubbing of Flat Surfaces," J. Appl. Phys., **24**(8), pp. 981–988.
[33] Luan, B., and Robbins, M. O., 2005, "The Breakdown of Continuum Models for Mechanical Contacts," Nature, **435**(7044), pp. 929–932.
[34] Luan, B., and Robbins, M. O., 2006, "Contact of Single Asperities With Varying Adhesion: Comparing Continuum Mechanics to Atomistic Simulations," Phys. Rev. E, **74**(2), p. 026111.
[35] Mo, Y., and Szlufarska, I., 2010, "Roughness Picture of Friction in Dry Nanoscale Contacts," Phys. Rev. B, **81**(3), p. 035405.
[36] Mo, Y., Turner, K. T., and Szlufarska, I., 2009, "Friction Laws at the Nanoscale," Nature, **457**(7233), pp. 1116–1119.
[37] Agrait, N., Yeyati, A. L., and Van Ruitenbeek, J. M., 2003, "Quantum Properties of Atomic-Sized Conductors," Phys. Rep., **377**(2–3), pp. 81–279.
[38] Gotsmann, B., and Lantz, M. A., 2013, "Quantized Thermal Transport Across Contacts of Rough Surfaces," Nat. Mater., **12**(1), pp. 59–65.
[39] Kopycinska-Müller, M., Geiss, R. H., and Hurley, D. C., 2006, "Contact Mechanics and Tip Shape in AFM-Based Nanomechanical Measurements," Ultramicroscopy, **106**(6), pp. 466–474.
[40] Carpick, R. W., Ogletree, D., and Salmeron, M., 1997, "Lateral Stiffness: A New Nanomechanical Measurement for the Determination of Shear Strengths With Friction Force Microscopy," Appl. Phys. Lett., **70**(12), pp. 1548–1555.
[41] Knoll, A. W., 2013, "Nanoscale Contact-Radius Determination by Spectral Analysis of Polymer Roughness Images," Langmuir, **29**(45), pp. 13958–13966.
[42] Slade, P. G., 2013, *Electrical Contacts: Principles and Applications*, CRC Press, Boca Raton, FL.
[43] Enachescu, M., van den Oetelaar, R., Carpick, R. W., Ogletree, D. F., Flipse, C., and Salmeron, M., 1998, "Atomic Force Microscopy Study of an Ideally Hard Contact: The Diamond(111)/Tungsten Carbide Interface," Phys. Rev. Lett., **81**(9), pp. 1877–1880.
[44] Enachescu, M., van den Oetelaar, R., Carpick, R. W., Ogletree, D. F., Flipse, C., and Salmeron, M., 1999, "Observation of Proportionality Between Friction and Contact Area at the Nanometer Scale," Tribol. Lett., **7**, pp. 73–78.
[45] Lantz, M. A., O'Shea, S. J., and Welland, M. E., 1997, "Simultaneous Force and Conduction Measurements in Atomic Force Microscopy," Phys. Rev. B, **56**(23), pp. 15345–15352.
[46] Bennewitz, R., Gyalog, T., Guggisberg, M., Bammerlin, M., Meyer, E., and Güntherodt, H. J., 1999, "Atomic-Scale Stick-Slip Processes on Cu(111)," Phys. Rev. B, **60**(16), pp. 301–304.
[47] Enachescu, M., 2004, "The Role of Contaminants in the Variation of Adhesion, Friction, and Electrical Conduction Properties of Carbide-Coated Scanning Probe Tips and Pt(111) in Ultrahigh Vacuum," J. Appl. Phys., **95**(12), p. 7694.
[48] Celano, U., Hantschel, T., Giammaria, G., Chintala, R. C., Conard, T., Bender, H., and Vandervorst, W., 2015, "Evaluation of the Electrical Contact Area in Contact-Mode Scanning Probe Microscopy," J. Appl. Phys., **117**(21), p. 214305.
[49] Marinello, F., Passeri, D., and Savio, E., 2013, *Acoustic Scanning Probe Microscopy*, Springer, Berlin.
[50] Johnson, K. L., 2011, *Contact Mechanics*, Cambridge University Press, Cambridge, UK.
[51] Oliver, W., and Pharr, G., 2004, "Measurement of Hardness and Elastic Modulus by Instrumented Indentation: Advances in Understanding and Refinements to Methodology," J. Mater. Res., **19**(3), pp. 3–20.
[52] Sneddon, I. N., 1965, "The Relation Between Load and Penetration in the Axisymmetric Boussinesq Problem for a Punch of Arbitrary Profile," Int. J. Eng. Sci., **3**(1), pp. 47–57.
[53] Pharr, G. M., Oliver, W. C., and Brotzen, F. R., 1992, "On the Generality of the Relationship Among Contact Stiffness, Contact Area, and Elastic-Modulus During Indentation," J. Mater. Res., **7**(3), pp. 613–617.
[54] Butt, H.-J., Cappella, B., and Kappl, M., 2005, "Force Measurements With the Atomic Force Microscope: Technique, Interpretation and Applications," Surf. Sci. Rep., **59**(1–6), pp. 1–152.
[55] Rabe, U., Amelio, S., Kopycinska, M., Hirsekorn, S., Kempf, M., Göken, M., and Arnold, W., 2002, "Imaging and Measurement of Local Mechanical Material Properties by Atomic Force Acoustic Microscopy," Surf. Interface Anal., **33**(2), pp. 65–70.
[56] Rabe, U., Amelio, S., Kester, E., Scherer, V., Hirsekorn, S., and Arnold, W., 2000, "Quantitative Determination of Contact Stiffness Using Atomic Force Acoustic Microscopy," Ultrasonics, **38**(1), pp. 430–437.
[57] Solares, S. D., and Chawla, G., 2010, "Frequency Response of Higher Cantilever Eigenmodes in Bimodal and Trimodal Tapping Mode Atomic Force Microscopy," Meas. Sci. Technol., **21**(12), p. 125502.
[58] Popov, V. L., 2010, *Contact Mechanics and Friction*, Springer, Berlin.
[59] Carpick, R. W., Agrait, N., Ogletree, D. F., and Salmeron, M., 1996, "Measurement of Interfacial Shear (Friction) With an Ultrahigh Vacuum Atomic Force Microscope," J. Vac. Sci. Technol. B, **14**(2), pp. 1289–1295.
[60] Akarapu, S., Sharp, T., and Robbins, M. O., 2011, "Stiffness of Contacts Between Rough Surfaces," Phys. Rev. Lett., **106**(20), p. 204301.
[61] Steiner, P., Roth, R., Gnecco, E., Glatzel, T., Baratoff, A., and Meyer, E., 2009, "Modulation of Contact Resonance Frequency Accompanying Atomic-Scale Stick–Slip in Friction Force Microscopy," Nanotechnology, **20**(49), p. 495701.
[62] Cheng, S., Luan, B., and Robbins, M. O., 2010, "Contact and Friction of Nanoasperities: Effects of Adsorbed Monolayers," Phys. Rev. E, **81**(1), p. 016102.
[63] Cattaneo, C., 1938, "Sul contatto di due corpi elastici: distribuzione locale degli sforzi," Rend. Accad. Naz. Lincei, **27**(6), pp. 342–348.
[64] Mindlin, R. D., 1949, "Compliance of Elastic Bodies in Contact," ASME J. Appl. Mech., **16**, p. 259.
[65] Mindlin, R. D., and Deresiewica, H., 1953, "Elastic Spheres in Contact Under Varying Oblique Forces," ASME J. Appl. Mech., **20**, p. 372.
[66] Sneddon, I. N., 1946, "Boussinesq's Problem for a Flat-Ended Cylinder," Math. Proc. Cambridge Philos. Soc., **42**(1), p. 29.
[67] Hanke, S., Petri, J., and Johannsmann, D., 2013, "Partial Slip in Mesoscale Contacts: Dependence on Contact Size," Phys. Rev. E, **88**(3), p. 032408.
[68] Carpick, R. W., Agrait, N., Ogletree, D. F., and Salmeron, M., 1996, "Variation of the Interfacial Shear Strength and Adhesion of a Nanometer-Sized Contact," Langmuir, **12**(13), pp. 3334–3340.
[69] Dietzel, D., Schwarz, U. D., and Schirmeisen, A., 2014, "Nanotribological Studies Using Nanoparticle Manipulation: Principles and Application to Structural Lubricity," Friction, **2**(2), pp. 114–139.
[70] Stoica, P., and Moses, R. L., 2005, *Spectral Analysis of Signals*, Prentice Hall, Upper Saddle River, NJ.
[71] Jacobs, T. D. B., Lunge, T., and Pastewka, L., 2017, "Quantitative Characterization of Surface Topography Using Spectral Analysis," Surf. Topogr.: Metrol. Prop., **5**(1), p. 013001.
[72] Jacobs, T. D. B., Wabiszewski, G. E., Goodman, A. J., and Carpick, R. W., 2016, "Characterizing Nanoscale Scanning Probes Using Electron Microscopy: A Novel Fixture and a Practical Guide," Rev. Sci. Instrum., **87**(1), p. 013703.

[73] Pohrt, R., and Popov, V. L., 2012, "Normal Contact Stiffness of Elastic Solids With Fractal Rough Surfaces," Phys. Rev. Lett., **108**(10), p. 104301.
[74] Khan, S. H., Matei, G., Patil, S., and Hoffmann, P. M., 2010, "Dynamic Solidification in Nanoconfined Water Films," Phys. Rev. Lett., **105**(10), p. 106101.
[75] Ovcharenko, A., Halperin, G., Etsion, I., and Varenberg, M., 2006, "A Novel Test Rig for In Situ and Real Time Optical Measurement of the Contact Area Evolution During Pre-Sliding of a Spherical Contact," Tribol. Lett., **23**(1), pp. 55–63.
[76] Ovcharenko, A., Halperin, G., and Etsion, I., 2008, "In Situ and Real-Time Optical Investigation of Junction Growth in Spherical Elastic–Plastic Contact," Wear, **264**(11–12), pp. 1043–1050.
[77] Krick, B. A., Vail, J. R., Persson, B., and Sawyer, W. G., 2012, "Optical In Situ Micro Tribometer for Analysis of Real Contact Area for Contact Mechanics, Adhesion, and Sliding Experiments," Tribol. Lett., **45**(1), pp. 185–194.
[78] Merkle, A. P., and Marks, L. D., 2008, "Liquid-Like Tribology of Gold Studied by In Situ TEM," Wear, **265**(11–12), pp. 1864–1869.
[79] Rodrigues, V., Fuhrer, T., and Ugarte, D., 2000, "Signature of Atomic Structure in the Quantum Conductance of Gold Nanowires," Phys. Rev. Lett., **85**(19), p. 4124.
[80] Alsem, D. H., Sood, S., Salmon, N., and Jacobs, T. D. B., 2016, "In Situ Electrical Testing of Device-Relevant Nanocontacts in the Transmission Electron Microscope," Microsc. Microanal., **22**(S3), pp. 818–819.
[81] Kizuka, T., 1998, "Atomic Process of Point Contact in Gold Studied by Time-Resolved High-Resolution Transmission Electron Microscopy," Phys. Rev. Lett., **81**(20), pp. 4448–4451.
[82] Kizuka, T., Yamada, K., Deguchi, S., Naruse, M., and Tanaka, N., 1997, "Cross-Sectional Time-Resolved High-Resolution Transmission Electron Microscopy of Atomic-Scale Contact and Noncontact-Type Scannings on Gold Surfaces," Phys. Rev. B, **55**(12), pp. 7398–7401.
[83] Kizuka, T., Ohmi, H., Sumi, T., Kumazawa, K., Deguchi, S., Naruse, M., Fujisawa, S., Sasaki, S., Yabe, A., and Enomoto, Y., 2001, "Simultaneous Observation of Millisecond Dynamics in Atomistic Structure, Force and Conductance on the Basis of Transmission Electron Microscopy," Jpn. J. Appl. Phys., **40**(2B), pp. L170–L173.
[84] Ohnishi, H., Kondo, Y., and Takayanagi, K., 1998, "Quantized Conductance Through Individual Rows of Suspended Gold Atoms," Nature, **395**(6704), pp. 780–783.
[85] Takayanagi, K., Kondo, Y., and Ohnishi, H., 2001, "Suspended Gold Nanowires: Ballistic Transport of Electrons," JSAP Int., **3**, pp. 3–8.
[86] Ishida, T., Sato, T., Ishikawa, T., Oguma, M., Itamura, N., Goda, K., Sasaki, N., and Fujita, H., 2014, "Time-Lapse Nanoscopy of Friction in the Non-Amontons and Non-Coulomb Regime," Nano Lett., **15**(3), pp. 1476–1480.
[87] Sato, T., Ishida, T., Jalabert, L., and Fujita, H., 2011, "Development of MEMS-in-TEM Setup to Observe Shear Deformation for the Study of Nano-Scale Friction," Tribol. Online, **6**(5), pp. 226–229.
[88] Jacobs, T. D. B., and Carpick, R. W., 2013, "Nanoscale Wear as a Stress-Assisted Chemical Reaction," Nat. Nanotechnol., **8**(2), pp. 108–112.
[89] Jacobs, T. D. B., Ryan, K. E., Keating, P. L., Grierson, D. S., Lefever, J. A., Turner, K. T., Harrison, J. A., and Carpick, R. W., 2013, "The Effect of Atomic-Scale Roughness on the Adhesion of Nanoscale Asperities: A Combined Simulation and Experimental Investigation," Tribol. Lett., **50**(1), pp. 81–93.
[90] Jacobs, T. D. B., Lefever, J. A., and Carpick, R. W., 2015, "A Technique for the Experimental Determination of the Length and Strength of Adhesive Interactions Between Effectively Rigid Materials," Tribol. Lett., **59**(1), pp. 1–11.
[91] Jacobs, T. D. B., Lefever, J. A., and Carpick, R. W., 2015, "Measurement of the Length and Strength of Adhesive Interactions in a Nanoscale Silicon–Diamond Interface," Adv. Mater. Interfaces, **2**(9), p. 1400547.
[92] Williams, D. B., and Carter, C. B., 2009, *Transmission Electron Microscopy: A Textbook for Materials Science*, Springer, Berlin.
[93] Zheng, K., Wang, C., Cheng, Y.-Q., Yue, Y., Han, X., Zhang, Z., Shan, Z., Mao, S. X., Ye, M., Yin, Y., and Ma, E., 2010, "Electron-Beam-Assisted Superplastic Shaping of Nanoscale Amorphous Silica," Nat. Commun., **1**(3), p. 24.
[94] Sarkar, R., Rentenberger, C., and Rajagopalan, J., 2015, "Electron Beam Induced Artifacts During In Situ TEM Deformation of Nanostructured Metals," Sci. Rep., **5**, p. 16345.
[95] Cheng, S., and Robbins, M. O., 2010, "Defining Contact at the Atomic Scale," Tribol. Lett., **39**(3), pp. 329–348.
[96] Daw, M. S., and Baskes, M. I., 1984, "Embedded-Atom Method: Derivation and Application to Impurities, Surfaces, and Other Defects in Metals," Phys. Rev. B, **29**(12), pp. 6443–6453.
[97] Foiles, S. M., Baskes, M. I., and Daw, M. S., 1986, "Embedded-Atom-Method Functions for the FCC Metals Cu, Ag, Au, Ni, Pd, Pt, and Their Alloys," Phys. Rev. B, **33**(12), pp. 7983–7991.
[98] Tersoff, J., 1988, "New Empirical Approach for the Structure and Energy of Covalent Systems," Phys. Rev. B, **37**(12), p. 6991.
[99] Stuart, S., Tutein, A., and Harrison, J. A., 2000, "A Reactive Potential for Hydrocarbons With Intermolecular Interactions," J. Chem. Phys., **112**(14), pp. 6472–6486.
[100] Becker, C. A., Tavazza, F., Trautt, Z. T., and de Macedo, R. A. B., 2013, "Considerations for Choosing and Using Force Fields and Interatomic Potentials in Materials Science and Engineering," Curr. Opin. Solid State Mater. Sci., **17**(6), pp. 277–283.
[101] Dong, Y., Li, Q., and Martini, A., 2013, "Molecular Dynamics Simulation of Atomic Friction: A Review and Guide," J. Vac. Sci. Technol. A, **31**(3), p. 030801.
[102] Li, L., Song, W., Xu, M., Ovcharenko, A., and Zhang, G., 2015, "Atomistic Insights Into the Loading–Unloading of an Adhesive Contact: A Rigid Sphere Indenting a Copper Substrate," Comput. Mater. Sci., **98**, pp. 105–111.
[103] Vishnubhotla, S. B., Chen, R., Khanal, S., Hu, X., Martini, A., and Jacobs, T. D. B., 2017, "Matching Atomistic Simulations and In Situ Experiments to Investigate the Mechanics of Nanoscale Contacts," Tribol. Lett. (submitted).
[104] Simmons, G., 1995, *Calculus With Analytic Geometry*, McGraw-Hill Education, New York.
[105] Hu, X., and Martini, A., 2015, "Atomistic Simulation of the Effect of Roughness on Nanoscale Wear," Comput. Mater. Sci., **102**(C), pp. 208–212.
[106] Ryan, K. E., Keating, P. L., Jacobs, T. D. B., Grierson, D. S., Turner, K. T., Carpick, R. W., and Harrison, J. A., 2014, "Simulated Adhesion Between Realistic Hydrocarbon Materials: Effects of Composition, Roughness, and Contact Point," Langmuir, **30**(8), pp. 2028–2037.
[107] Gao, G., Cannara, R., Carpick, R. W., and Harrison, J. A., 2007, "Atomic-Scale Friction on Diamond: A Comparison of Different Sliding Directions on (001) and (111) Surfaces Using MD and AFM," Langmuir, **23**(10), pp. 5394–5405.
[108] Chandross, M., Lorenz, C. D., Stevens, M. J., and Grest, G. S., 2008, "Simulations of Nanotribology With Realistic Probe Tip Models," Langmuir, **24**(4), pp. 1240–1246.
[109] Chandross, M., Grest, G. S., and Stevens, M. J., 2002, "Friction Between Alkylsilane Monolayers: Molecular Simulation of Ordered Monolayers," Langmuir, **18**(22), pp. 8392–8399.
[110] Liu, X. Z., Ye, Z., Dong, Y., Egberts, P., Carpick, R. W., and Martini, A., 2015, "Dynamics of Atomic Stick-Slip Friction Examined With Atomic Force Microscopy and Atomistic Simulations at Overlapping Speeds," Phys. Rev. Lett., **114**(14), p. 146102.
[111] Jiang, Y., Harrison, J. A., Schall, J. D., Ryan, K. E., Carpick, R. W., and Turner, K. T., 2017, "Correcting for Tip Geometry Effects in Molecular Simulations of Single-Asperity Contact," Tribol. Lett., **65**(3), p. 78.
[112] Hu, X., Altoe, M. V., and Martini, A., 2017, "Amorphization-Assisted Nanoscale Wear During the Running-In Process," Wear, **370–371**, pp. 46–50.
[113] Pearson, J. D., Gao, G., Zikry, M. A., and Harrison, J. A., 2009, "Nanoindentation of Model Diamond Nanocomposites: Hierarchical Molecular Dynamics and Finite-Element Simulations," Comput. Mater. Sci., **47**(1), pp. 1–11.
[114] Brukman, M. J., Gao, G., Nemanich, R. J., and Harrison, J. A., 2008, "Temperature Dependence of Single-Asperity Diamond–Diamond Friction Elucidated Using AFM and MD Simulations," J. Phys. Chem. C, **112**(25), pp. 9358–9369.
[115] Brunetto, G., and Martini, A., 2017, "Atomistic Description of Coupled Thermal-Mechanical Stresses on a Gold/HOPG Nanocontact," Comput. Mater. Sci., **130**, pp. 165–171.
[116] Adelman, S. A., 1976, "Generalized Langevin Equation Approach for Atom/Solid-Surface Scattering: General Formulation for Classical Scattering Off Harmonic Solids," J. Chem. Phys., **64**(6), p. 2375.
[117] Hoover, W. G., 1985, "Canonical Dynamics: Equilibrium Phase-Space Distributions," Phys. Rev. A, **31**(3), pp. 1695–1697.
[118] Pastewka, L., Moser, S., and Moseler, M., 2010, "Atomistic Insights Into the Running-In, Lubrication, and Failure of Hydrogenated Diamond-Like Carbon Coatings," Tribol. Lett., **39**(1), pp. 49–61.
[119] Soddemann, T., Dünweg, B., and Kremer, K., 2003, "Dissipative Particle Dynamics: A Useful Thermostat for Equilibrium and Nonequilibrium Molecular Dynamics Simulations," Phys. Rev. E, **68**(4), p. 046702.
[120] Peters, E. A. J. F., 2004, "Elimination of Time Step Effects in DPD," Europhys. Lett., **66**(3), p. 311.
[121] Pastewka, L., Moser, S., Gumbsch, P., and Moseler, M., 2010, "Anisotropic Mechanical Amorphization Drives Wear in Diamond," Nat. Mater., **10**(1), pp. 34–38.
[122] Martini, A., Dong, Y., Perez, D., and Voter, A. F., 2009, "Low-Speed Atomistic Simulation of Stick–Slip Friction Using Parallel Replica Dynamics," Tribol. Lett., **36**(1), pp. 63–68.
[123] Perez, D., Dong, Y., Martini, A., and Voter, A. F., 2010, "Rate Theory Description of Atomic Stick-Slip Friction," Phys. Rev. B, **81**(24), p. 245415.
[124] Knippenberg, M., Mikulski, P., Dunlap, B., and Harrison, J. A., 2008, "Atomic Contributions to Friction and Load for Tip–Self-Assembled Monolayers Interactions," Phys. Rev. B, **78**(23), p. 235409.
[125] Solhjoo, S., and Vakis, A. I., 2015, "Definition and Detection of Contact in Atomistic Simulations," Comput. Mater. Sci., **109**, pp. 172–182.
[126] Burnham, N. A., Colton, R. J., and Pollock, H. M., 1991, "Interpretation Issues in Force Microscopy," J. Vac. Sci. Technol. A, **9**(4), pp. 2548–2510.
[127] Li, S., Li, Q., Carpick, R. W., Gumbsch, P., Liu, X. Z., Ding, X., Sun, J., and Li, J., 2016, "The Evolving Quality of Frictional Contact With Graphene," Nature, **539**(7630), pp. 541–545.
[128] Spijker, P., Anciaux, G., and Molinari, J.-F., 2012, "The Effect of Loading on Surface Roughness at the Atomistic Level," Comput. Mech., **50**(3), pp. 273–283.
[129] Eder, S., Vernes, A., Vorlaufer, G., and Betz, G., 2011, "Molecular Dynamics Simulations of Mixed Lubrication With Smooth Particle Post-Processing," J. Phys.: Condens. Matter, **23**(17), p. 175004.
[130] Cha, P.-R., Srolovitz, D. J., and Vanderlick, T. K., 2004, "Molecular Dynamics Simulation of Single Asperity Contact," Acta Mater., **55**(13), pp. 3983–3996.
[131] Rubio, G., Agrait, N., and Vieira, S., 1996, "Atomic-Sized Metallic Contacts: Mechanical Properties and Electronic Transport," Phys. Rev. Lett., **76**(13), pp. 2302–2305.

[132] Maugis, D., 2000, *Contact, Adhesion and Rupture of Elastic Solids*, Springer, Berlin.
[133] Maugis, D., 1992, "Adhesion of Spheres: The JKR-DMT Transition Using a Dugdale Model," J. Colloid Interface Sci., **150**(1), pp. 243–269.
[134] Grierson, D., Flater, E., and Carpick, R., 2005, "Accounting for the JKR-DMT Transition in Adhesion and Friction Measurements With Atomic Force Microscopy," J. Adhes. Sci. Technol., **19**(3–5), pp. 291–311.
[135] Hertz, H., 1881, "On the Contact of Elastic Solids," J. Reine Angew. Math., **92**(156–171), p. 110.
[136] Derjaguin, B. V., Muller, V. M., and Toporov, Y. P., 1975, "Effect of Contact Deformations on the Adhesion of Particles," J. Colloid Interface Sci., **53**(2), pp. 314–326.
[137] Johnson, K. L., Kendall, K., and Roberts, A. D., 1971, "Surface Energy and the Contact of Elastic Solids," Proc. R. Soc. A, **324**(1558), pp. 301–313.
[138] Tabor, D., 1977, "Surface Forces and Surface Interactions," J. Colloid Interface Sci., **58**(1), pp. 2–13.
[139] Carpick, R. W., Ogletree, D. F., and Salmeron, M., 1999, "A General Equation for Fitting Contact Area and Friction Vs Load Measurements," J. Colloid Interface Sci., **211**(2), pp. 395–400.
[140] Zheng, Z., and Yu, J., 2007, "Using the Dugdale Approximation to Match a Specific Interaction in the Adhesive Contact of Elastic Objects," J. Colloid Interface Sci., **310**(1), pp. 27–34.
[141] Grierson, D. S., Liu, J., Carpick, R. W., and Turner, K. T., 2013, "Adhesion of Nanoscale Asperities With Power-Law Profiles," J. Mech. Phys. Solids, **61**(2), pp. 597–610.
[142] Willis, J. R., 1966, "Hertzian Contact of Anisotropic Bodies," J. Mech. Phys. Solids, **14**(3), pp. 163–176.
[143] Turner, J. R., 1980, "Contact on a Transversely Isotropic Half-Space, or Between Two Transversely Isotropic Bodies," Int. J. Solids Struct., **16**(5), pp. 409–419.
[144] Swanson, S. R., 2004, "Hertzian Contact of Orthotropic Materials," Int. J. Solids Struct., **41**(7), pp. 1945–1959.
[145] Hsueh, C. H., and Miranda, P., 2004, "Master Curves for Hertzian Indentation on Coating/Substrate Systems," J. Mater. Res., **19**(1), pp. 94–100.
[146] Reedy, E. D., 2006, "Thin-Coating Contact Mechanics With Adhesion," J. Mater. Res., **21**(10), pp. 2660–2668.
[147] Reedy, E. D., 2017, "Contact Mechanics for Coated Spheres That Includes the Transition From Weak to Strong Adhesion," J. Mater. Res., **22**(9), pp. 2617–2622.
[148] Fischer-Cripps, A. C., 2000, "A Review of Analysis Methods for Sub-Micron Indentation Testing," Vacuum, **58**(4), pp. 569–585.
[149] Gouldstone, A., Chollacoop, N., Dao, M., Li, J., Minor, A. M., and Shen, Y.-L., 2007, "Indentation Across Size Scales and Disciplines: Recent Developments in Experimentation and Modeling," Acta Mater., **55**(12), pp. 4015–4039.
[150] Schwarz, U. D., Zworner, O., Koster, P., and Wiesendanger, P., 1997, "Quantitative Analysis of the Frictional Properties of Solid Materials at Low Loads—II: Mica and Germanium Sulfide," Phys. Rev. B, **56**(11), pp. 6997–7000.
[151] Schwarz, U. D., Zworner, O., Koster, P., and Wiesendanger, R., 1997, "Quantitative Analysis of the Frictional Properties of Solid Materials at Low Loads—I: Carbon Compounds," Phys. Rev. B, **56**(11), pp. 6987–6996.
[152] Lessel, M., Loskill, P., Hausen, F., Gosvami, N. N., Bennewitz, R., and Jacobs, K., 2013, "Impact of van der Waals Interactions on Single Asperity Friction," Phys. Rev. Lett., **111**(3), p. 035502.
[153] Carbone, G., and Bottiglione, F., 2008, "Asperity Contact Theories: Do They Predict Linearity Between Contact Area and Load?," J. Mech. Phys. Solids, **56**(8), pp. 2555–2572.
[154] Yastrebov, V. A., Anciaux, G., and Molinari, J.-F., 2014, "The Contact of Elastic Regular Wavy Surfaces Revisited," Tribol. Lett., **56**(1), pp. 171–183.
[155] Ciavarella, M., Murolo, C., and Demelio, G., 2006, "On the Elastic Contact of Rough Surfaces: Numerical Experiments and Comparisons With Recent Theories," Wear, **261**(10), pp. 1102–1113.
[156] Jackson, R. L., and Green, I., 2011, "On the Modeling of Elastic Contact Between Rough Surfaces," Tribol. Trans., **54**(2), pp. 300–314.
[157] Archard, J. F., 1957, "Elastic Deformation and the Laws of Friction," Proc. R. Soc. A, **243**(1233), pp. 190–205.
[158] Greenwood, J. A., and Tripp, J. H., 1970, "The Contact of Two Nominally Flat Rough Surfaces," Proc. Inst. Mech. Eng., **185**(1), pp. 625–633.
[159] McCool, J. I., 1992, "Non-Gaussian Effects in Microcontact," Int. J. Mach. Tools Manuf., **32**(1–2), pp. 115–123.
[160] Kotwal, C. A., and Bhushan, B., 1996, "Contact Analysis of Non-Gaussian Surfaces for Minimum Static and Kinetic Friction and Wear," Tribol. Trans., **39**(4), pp. 890–898.
[161] McCool, J. I., 2000, "Extending the Capability of the Greenwood Williamson Microcontact Model," ASME J. Tribol., **122**(3), pp. 496–502.
[162] Bush, A. W., and Gibson, R. D., 1975, "The Elastic Contact of a Rough Surface," Wear, **35**(1), pp. 87–111.
[163] Bush, A. W., Gibson, R. D., and Keogh, G. P., 1979, "Strongly Anisotropic Rough Surfaces," ASME J. Tribol., **101**(1), pp. 15–20.
[164] Nayak, P. R., 1971, "Random Process Model of Rough Surfaces," J. Lubr. Technol., **93**(3), p. 398.
[165] Yastrebov, V. A., Anciaux, G., and Molinari, J. F., 2015, "From Infinitesimal to Full Contact Between Rough Surfaces: Evolution of the Contact Area," Int. J. Solids Struct., **52**, pp. 83–102.
[166] Benz, M., Rosenberg, K. J., Edward J Kramer, A., and Israelachvili, J. N., 2006, "The Deformation and Adhesion of Randomly Rough and Patterned Surfaces," J. Phys. Chem. B, **110**(24), pp. 11884–11893.
[167] Carbone, G., Lorenz, B., and Persson, B. N. J., 2009, "Contact Mechanics and Rubber Friction for Randomly Rough Surfaces With Anisotropic Statistical Properties," Eur. Phys. J. E, **29**(3), pp. 275–284.
[168] Lorenz, B., Carbone, G., and Schulze, C., 2010, "Average Separation Between a Rough Surface and a Rubber Block: Comparison Between Theories and Experiments," Wear, **268**(7–8), pp. 984–990.
[169] Carbone, G., Scaraggi, M., and Tartaglino, U., 2009, "Adhesive Contact of Rough Surfaces: Comparison Between Numerical Calculations and Analytical Theories," Eur. Phys. J. E, **30**, pp. 65–74.
[170] DelRio, F. W., de Boer, M. P., Knapp, J. A., David Reedy, E., Clews, P. J., and Dunn, M. L., 2005, "The Role of Van Der Waals Forces in Adhesion of Micromachined Surfaces," Nat. Mater., **4**(8), pp. 629–634.
[171] Tayebi, N., and Polycarpou, A. A., 2005, "Reducing the Effects of Adhesion and Friction in Microelectromechanical Systems (MEMSs) Through Surface Roughening: Comparison Between Theory and Experiments," J. Appl. Phys., **98**(7), p. 073528.
[172] Greenwood, J. A., 1984, "A Unified Theory of Surface-Roughness," Proc. R. Soc. A, **393**(1804), pp. 133–157.
[173] Bowden, F. P., and Tabor, D., 2001, *The Friction and Lubrication of Solids*, Oxford University Press, Oxford, UK.
[174] Longuet-Higgins, M. S., 1957, "The Statistical Analysis of a Random, Moving Surface," Philos. Trans. R. Soc. London, Ser. A, **249**(966), pp. 321–387.
[175] Whitehouse, D. J., and Archard, J. F., 1970, "The Properties of Random Surfaces of Significance in Their Contact," Proc. R. Soc. A, **316**(1524), pp. 97–121.
[176] Mandelbrot, B. B., and Pignoni, R., 1983, *The Fractal Geometry of Nature*, WH Freeman, New York.
[177] Persson, B. N. J., Albohr, O., Tartaglino, U., Volokitin, A. I., and Tosatti, E., 2004, "On the Nature of Surface Roughness With Application to Contact Mechanics, Sealing, Rubber Friction and Adhesion," J. Phys.: Condens. Matter, **17**(1), pp. R1–R62.
[178] Mandelbrot, B. B., Passoja, D. E., and Paullay, A. J., 1984, "Fractal Character of Fracture Surfaces of Metals," Nature, **308**(5961), pp. 721–722.
[179] Majumdar, A., and Bhushan, B., 1990, "Role of Fractal Geometry in Roughness Characterization and Contact Mechanics of Surfaces," ASME J. Tribol., **112**(2), pp. 205–216.
[180] Ganti, S., and Bhushan, B., 1995, "Generalized Fractal Analysis and Its Applications to Engineering Surfaces," Wear, **180**(1–2), pp. 17–34.
[181] Bonamy, D., Ponson, L., Prades, S., Bouchaud, E., and Guillot, C., 2006, "Scaling Exponents for Fracture Surfaces in Homogeneous Glass and Glassy Ceramics," Phys. Rev. Lett., **97**(13), p. 135504.
[182] Ponson, L., Bonamy, D., and Bouchaud, E., 2006, "Two-Dimensional Scaling Properties of Experimental Fracture Surfaces," Phys. Rev. Lett., **96**(3), p. 035506.
[183] Persson, B. N. J., 2001, "Theory of Rubber Friction and Contact Mechanics," J. Chem. Phys., **115**(8), p. 3840.
[184] Dieterich, J. H., and Kilgore, B. D., 1996, "Imaging Surface Contacts: Power Law Contact Distributions and Contact Stresses in Quartz, Calcite, Glass and Acrylic Plastic," Tectonophysics, **256**(1–4), pp. 219–239.
[185] Hyun, S., Pei, L., Molinari, J. F., and Robbins, M. O., 2004, "Finite-Element Analysis of Contact Between Elastic Self-Affine Surfaces," Phys. Rev. E, **70**(2), p. 026117.
[186] Amontons, G., 1699, "De la resistance causee dansles machines," Mem. de l'Academie Royal A.
[187] Persson, B. N. J., 2002, "Adhesion Between Elastic Bodies With Randomly Rough Surfaces," Phys. Rev. Lett., **89**(24), p. 245502.
[188] Persson, B. N. J., and Tosatti, E., 2001, "The Effect of Surface Roughness on the Adhesion of Elastic Solids," J. Chem. Phys., **115**(12), p. 5597.
[189] Peressadko, A., Hosoda, N., and Persson, B. N. J., 2005, "Influence of Surface Roughness on Adhesion Between Elastic Bodies," Phys. Rev. Lett., **95**(12), p. 124301.
[190] Persson, B. N. J., 2008, "Capillary Adhesion Between Elastic Solids With Randomly Rough Surfaces," J. Phys.: Condens. Matter, **20**(31), p. 315007.
[191] Scaraggi, M., and Persson, B. N. J., 2015, "Friction and Universal Contact Area Law for Randomly Rough Viscoelastic Contacts," J. Phys.: Condens. Matter, **27**(10), p. 105102.
[192] Pastewka, L., and Robbins, M. O., 2014, "Contact Between Rough Surfaces and a Criterion for Macroscopic Adhesion," Proc. Natl. Acad. Sci., **111**(9), pp. 3298–3303.
[193] Mulakaluri, N., and Persson, B. N. J., 2011, "Adhesion Between Elastic Solids With Randomly Rough Surfaces: Comparison of Analytical Theory With Molecular-Dynamics Simulations," Europhys. Lett., **96**(6), p. 66003.
[194] Rabinovich, Y., 2000, "Adhesion Between Nanoscale Rough Surfaces—I: Role Asperity Geometry," J. Colloid Interface Sci., **232**(1), pp. 10–16.
[195] Rabinovich, Y., 2000, "Adhesion Between Nanoscale Rough Surfaces—II: Measurement and Comparison With Theory," J. Colloid. Interface Sci., **232**(1), pp. 17–24.
[196] Katainen, J., Paajanen, M., Ahtola, E., Pore, V., and Lahtinen, J., 2006, "Adhesion as an Interplay Between Particle Size and Surface Roughness," J. Colloid. Interface Sci., **304**(2), pp. 524–529.
[197] Ramakrishna, S. N., Clasohm, L. Y., Rao, A., and Spencer, N. D., 2011, "Controlling Adhesion Force by Means of Nanoscale Surface Roughness," Langmuir, **27**(16), pp. 9972–9978.
[198] Jiang, Y., and Turner, K. T., 2016, "Measurement of the Strength and Range of Adhesion Using Atomic Force Microscopy," Extreme Mech. Lett., **9**(Pt. 1), pp. 119–126.
[199] Pastewka, L., and Robbins, M. O., 2016, "Contact Area of Rough Spheres: Large Scale Simulations and Simple Scaling Laws," Appl. Phys. Lett., **108**(22), p. 221601.

[200] Spijker, P., Anciaux, G., and Molinari, J.-F., 2013, "Relations Between Roughness, Temperature and Dry Sliding Friction at the Atomic Scale," Tribol. Int., **59**, pp. 222–229.
[201] Campañá, C., and Müser, M. H., 2007, "Contact Mechanics of Real Vs. Randomly Rough Surfaces: A Green's Function Molecular Dynamics Study," Europhys. Lett., **77**(3), p. 38005.
[202] Eder, S. J., Feldbauer, G., Bianchi, D., Cihak-Bayr, U., Betz, G., and Vernes, A., 2015, "Applicability of Macroscopic Wear and Friction Laws on the Atomic Length Scale," Phys. Rev. Lett., **115**(2), p. 025502.
[203] Pastewka, L., Prodanov, N., Lorenz, B., Müser, M. H., Robbins, M. O., and Persson, B. N. J., 2013, "Finite-Size Scaling in the Interfacial Stiffness of Rough Elastic Contacts," Phys. Rev. E, **87**(6), p. 062809.
[204] Putignano, C., Afferrante, L., Carbone, G., and Demelio, G., 2012, "The Influence of the Statistical Properties of Self-Affine Surfaces in Elastic Contacts: A Numerical Investigation," J. Mech. Phys. Solids, **60**(5), pp. 973–982.
[205] Prodanov, N., Dapp, W. B., and Müser, M. H., 2014, "On the Contact Area and Mean Gap of Rough, Elastic Contacts: Dimensional Analysis, Numerical Corrections, and Reference Data," Tribol. Lett., **53**(2), pp. 433–448.
[206] Yanson, A. I., Bollinger, G. R., Van den Brom, H. E., Agrait, N., and Van Ruitenbeek, J. M., 1998, "Formation and Manipulation of a Metallic Wire of Single Gold Atoms," Nature, **395**(6704), pp. 783–785.
[207] Jarvis, S. P., Lantz, M. A., Ogiso, H., Tokumoto, H., and Dürig, U., 1999, "Conduction and Mechanical Properties of Atomic Scale Gold Contacts," Appl. Phys. Lett., **75**(20), p. 3132.
[208] Landman, U., Luedtke, W. D., Burnham, N., and Colton, R., 1990, "Atomistic Mechanisms and Dynamics of Adhesion, Nanoindentation, and Fracture," Science, **248**(4954), pp. 454–461.
[209] Sutton, A. P., and Pethica, J. B., 1990, "Inelastic Flow Processes in Nanometre Volumes of Solids," J. Phys.: Condens. Matter, **2**(24), p. 5317.
[210] Song, J., and Srolovitz, D. J., 2008, "Mechanism for Material Transfer in Asperity Contact," J. Appl. Phys., **104**(12), p. 124312.
[211] Yong, C. W., Smith, W., and Kendall, K., 2003, "Molecular Dynamics Simulations of (001) MgO Surface Contacts: Effects of Tip Structures and Surface Matching," Nanotechnology, **14**, pp. 829–839.
[212] Fortini, A., Mendelev, M. I., Buldyrev, S., and Srolovitz, D., 2008, "Asperity Contacts at the Nanoscale: Comparison of Ru and Au," J. Appl. Phys., **104**(7), p. 074320.
[213] Yang, L., and Martini, A., 2013, "Nano-Scale Roughness Effects on Hysteresis in Micro-Scale Adhesive Contact," Tribol. Int., **58**, pp. 40–46.
[214] Todorov, T. N., and Sutton, A. P., 1996, "Force and Conductance Jumps in Atomic-Scale Metallic Contacts," Phys. Rev. B, **54**(20), p. R14234.
[215] Dednam, W., Sabater, C., Fernandez, M. A., Untiedt, C., Palacios, J. J., and Caturla, M. J., 2015, "Modeling Contact Formation Between Atomic-Sized Gold Tips Via Molecular Dynamics," J. Phys.: Conf. Ser., **574**, p. 012045.